Shock Effects in Meteorites

Thomas G. Sharp
Arizona State University

Paul S. DeCarli
SRI International

1. INTRODUCTION

Shock waves have played an important role in the history of virtually all meteorites. All models of the early solar system invoke condensation of mineral grains, aggregation of grains to form small bodies, and aggregation of most of the small bodies to form planets. The remaining small bodies, the asteroids, are accepted as the source of most meteorites. Throughout the history of the solar system, these small bodies have repeatedly collided with one another and with the planets. Since collisions produce shock waves in the colliding bodies, an understanding of shock wave effects is important to unraveling the impact history of the solar system as it is revealed in meteorites.

This chapter was originally intended as an update of the chapter by *Stöffler et al.* (1988). Rather than update that chapter, which relies heavily on laboratory shock-recovery experiments in the interpretation of shock effects in meteorites, we have decided to take a different approach. Here we emphasize the use of static high-pressure data on phase equilibria together with shock wave and thermal physics calculations to interpret observed microstructures of shocked meteorites. A number of papers published during the past ten years have shown that this approach can yield new insights on the impact history of meteorites (*Chen et al.,* 1996, 2004b; *Sharp et al.,* 1997; *Langenhorst and Poirier,* 2000a; *Xie and Sharp,* 2000, 2004; *Xie et al.,* 2002, 2005; *DeCarli et al.,* 2004; *Beck et al.,* 2004, 2005; *Ohtani et al.,* 2004). One requirement for use of this approach is that some knowledge of shock wave physics is required. Most general articles on shock wave physics do not present the information in a way that is useful to a reader who has been primarily trained in geology or mineralogy.

One of the objectives of this chapter is to present a useful tutorial on shock waves and shock wave calculations, including shock temperature and postshock temperature calculations. Our emphasis is on simple techniques and useful approximations rather than mathematical rigor. We will even attempt to present simple explanations of complicated phenomena, such as the quasichaotic nature of shock propagation in heterogeneous and/or porous materials. We also present examples to illustrate how the principles of shock wave and thermal physics may be used to interpret the history of naturally shocked materials and how the occurrences and formation mechanisms of high-pressure minerals in meteorites can be used to constrain shock pressures.

2. BACKGROUND

Shock wave effects on materials have been studied for centuries, ever since the invention of the cannon. Military engineers, concerned either with protecting or destroying structures (e.g., castles, forts, ships, armored vehicles), studied semiempirical correlation between impact damage and both target and projectile parameters, e.g., target dimensions and strength, impact velocity, projectile shape, projectile strength, etc. In a parallel effort, physicists were attempting to gain a good theoretical understanding of shock wave propagation in solids. The theoretical approach begins with simplification of the problem, e.g., the assumption that the material is homogeneous and can be treated as a continuum. Additional simplifications, e.g., assuming one-dimensional planar flow and neglecting material strength, lead to a theory of shock wave propagation based on Newton's laws of motion and on classical thermodynamics. The continuum theory and its historical development are covered in *Courant and Friedrichs* (1948). However, those of us who use high-resolution tools to study shock wave effects in materials may find it difficult to reconcile our observations of localized shock effects with continuum theories.

Shock propagation in a heterogeneous material, such as a meteorite, is an extraordinarily complex process when examined on the submicrometer scale of our observational tools. Because the shock properties of meteoritic minerals span a wide range, the initial nanoseconds of shock propagation through the meteorite appear chaotic. The initial peak pressure in the shock front can vary by as much as an order of magnitude from grain to grain or even within a single mineral grain, depending on details of the local environment. One consequence of that chaotic pressure distribution is that the shock temperature distribution is also chaotic. As we will show later, the shock temperature can also vary by as much as an order of magnitude between grains and even within a single grain. Pressure equilibration is achieved rapidly, on the timescale of the elastic wave transit time through the larger mineral grains. For a typical chondrite, having millimeter-sized grains, pressure equilibration will be complete within about a microsecond after arrival of the initial shock. In contrast, millimeter-scale temperature heterogeneities equilibrate on a timescale of seconds.

The studies by Kieffer and co-workers (*Kieffer,* 1971; *Kieffer et al.,* 1976) of shocked Coconino sandstone from Meteor Crater, Arizona, detail the complexity of shock in-

teractions on a submicrometer scale. They observed the intermixture of quartz, coesite, and stishovite within small areas and noted that no equilibrium P–T–V conditions exist where all three phases are simultaneously stable. They state: "The coexistence of these phases across regions of less than a thousand Angstroms in diameter indicates great variations of pressure and temperature locally within the shock, or nonequilibrium reaction conditions, or both."

For the most part, shock wave researchers have been able to ignore the complications of initial shock pressure equilibration in heterogeneous materials by using measurement techniques that average over the local fluctuations. This approach of using a continuum model to study shock wave propagation in porous and/or heterogeneous materials is generally satisfactory when one is concerned with centimeter-scale phenomena. Thus, the term "peak pressure," as it is customarily used, refers to the averaged peak pressure rather than to the nanosecond-duration peaks localized in submillimeter-sized regions. In the interest of facilitating interdisciplinary communication, we shall use the term "peak pressure" in its customary sense. In the absence of accepted terminology we use the terms "transient" and "spike" to refer to the nanoseconds-duration initial peak. Following common practice among shock wave researches, we use the term "ring down" to describe the complex series of shock interactions by which an initial high-pressure spike equilibrates to a lower pressure. Similarly, the term "ring up" describes a process beginning at a low pressure and equilibrating at a higher pressure.

As we will show later, shock temperature is sensitive to the detailed loading path experienced by the material during the initial pressure equilibration phase. Consider two feldspar grains in a chondrite. Depending on details such as the geometry and mineralogy of nearby grains, one feldspar grain may experience an initial low pressure that "rings up" to equilibrium and the second grain may experience an initial high-pressure spike that "rings down" to equilibrium. The difference in shock temperatures could be more than a factor of 2. In the case of a short-duration shock, one grain could be solid on release of pressure, whereas the other grain would be molten.

With the evolution of computer methods and capabilities, it has become possible to begin modeling shock wave propagation in real heterogeneous materials. New experimental techniques, including high-spatial-resolution dynamic measurements, permit detailed comparison of experiments with three-dimensional calculations (*Baer and Trott,* 2002, 2004). The goal of modern shock wave researchers is to develop a first-principles understanding of shock wave propagation valid on all scales from the atomic upward (*Gupta,* 2002; *Asay,* 2002).

The term "microscale modeling" is used to describe atomic and molecular scale modeling. Computational modeling on the micrometer scale, the scale of interest to meteorite researchers, must therefore be called "mesoscale modeling." Baer and co-workers have described mesoscale three-dimensional calculations of shock wave propagation in simple heterogeneous materials (*Baer,* 2000; *Baer and Trott,* 2002). Extraordinary computer capability was required to cope with 5-μm cell sizes and nanosecond time steps. One calculation indicated that the process of equilibrating to a "peak pressure" of 3 GPa involved nanosecond-duration transient spikes of over 30 GPa in the model heterogeneous material. One might suggest that these calculations confirm Kieffer's inference of great local variations of pressure and temperature in the initial stages of shock compression of a heterogeneous material. However, it would be more appropriate to state that the calculations are validated by Kieffer's work. Her observations had a spatial resolution at least 2 orders of magnitude higher than Baer's calculations. Kieffer also noted that the effective shock pressure duration in her samples was in the range of tens of milliseconds. Baer's calculations cover only the time required for pressure equilibration, generally less that a microsecond. Although calculations of pressure equilibration in heterogeneous materials require a supercomputer, independent thermal equilibration calculations can be performed on a modest personal computer.

This paper concentrates on the effects of shock pressures *per se*. However, we must mention that much current research is concerned with understanding phenomena, including fracture and plastic deformation, that occur during release of pressure. These phenomena should be of interest to students of meteorites who wonder why many shocked chondrites are so large and so strong. The usual result of shock loading experiments on nonporous rocks is fragmentation into submillimeter-sized pieces. This is the case even when extreme care is taken to use matched impedance momentum traps (*Hörz,* 1968). The wave interactions that result in fracture are associated with rapid release of pressure. One would expect that fragmentation and fracture would be minimized by a relatively slow release of pressure. We know from shock wave theory that the rate of pressure release will vary inversely with distance from a free surface. Thus it appears that appropriate application of dynamic fracture studies could yield further details, such as depth of a meteorite below the surface of a parent body at the time of a major impact. Recent books by *Nesterenko* (2001) and *Antoun et al.* (2003) summarize current knowledge of dynamic deformation and fracture. The book by *Meyers* (1994) is an excellent introduction to the field.

2.1. Elementary Shock Wave Theory and Calculations

Most review articles on shock wave physics take a rigorous approach toward interpretation of the physics of very simple geometries, e.g., planar impact or spherical flow in a homogeneous material. Here we attempt to present a simple, nonrigorous discussion of the complexities of shock wave propagation in a polymineralic and possibly cracked or porous rock. We also present approximate spreadsheet-based techniques for calculation of postshock temperature and shock temperature. For a rigorous analysis and deriva-

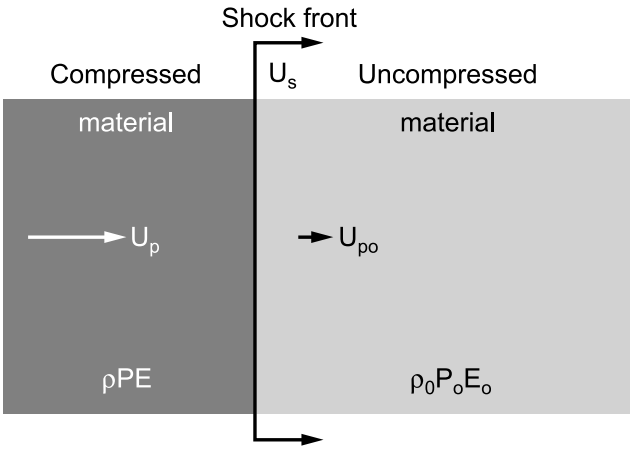

Fig. 1. Planar shock wave in a material.

tion of equations, the reader may consult various standard references (*Courant and Friedrichs,* 1948; *McQueen et al.,* 1970; *Duvall and Fowles,* 1963; *Melosh,* 1989; *Migault,* 1998). The graphical techniques and simplifying assumptions presented in this section are familiar to most shock wave specialists, who still use them to verify that complex computer codes running on supercomputers are giving "reasonable" results.

We begin with Fig. 1, the standard one-dimensional planar shock diagram illustrating the thermodynamic state variables and the Rankine Hugoniot equations. The state variables are pressure P, specific volume V ($V = 1/\rho$), and internal energy E. P_o, V_o, (or ρ_0), and E_o are the values of these variables in the unshocked state. P, V (or ρ), and E are the values in the shocked state. A shock wave is characterized by the kinetic variables U_s, shock velocity, and U_p, particle velocity.

From conservation of mass,

$$\rho(U_s - U_p) = \rho_0 U_s \quad (1)$$

From conservation of momentum,

$$P - P_o = \rho_0 U_s U_p \quad (2)$$

From conservation of energy,

$$PU_p = \rho_0 U_s(E - E_o) + (1/2)\rho_0 U_p^2 U_s \quad (3)$$

These equations may be rewritten as

$$U_p^2 = (P - P_o)(V_o - V) \quad (4)$$

$$U_s^2 = V_o^2(P - P_o)/(V_o - V) \quad (5)$$

$$E - E_o = (1/2)\,(P + P_o)(V_o - V) \quad (6)$$

There are three equations in five unknowns, P, V, U_s, U_p, and E. With a fourth relationship between any two of the variables one may completely define the shock state. This fourth relationship is the equation of state of the material. The equation of state may be represented in a variety of equivalent forms: As relationships in the P–V plane, in the P–U_s plane, in the P–U_p plane, or in the U_s–U_p plane. P–U_p representations are useful when calculating interface pressures between different materials. P–V representations are useful when making approximate calculations of shock and postshock temperatures (or internal energy changes).

However, shock wave equations of state (Hugoniots) are most often presented as relationships between U_s, shock velocity, and U_p, particle velocity, in the form

$$U_s = C_o + sU_p \quad (7)$$

McQueen (1964) originally presented Hugoniot data in this form because shock velocity was directly measured and particle velocity was inferred from the measured free surface velocity, Ufs. In the absence of phase transitions, $U_p \sim U_{fs}/2$ (*Walsh and Christian,* 1955). *McQueen* (1964) also noted that the relationship between U_s and U_p, for most materials, is linear over a large range of pressures. Deviations from linearity are often a sign of complexity in material response, e.g., phase transitions. In some cases, the deviations from linearity may be handled by the addition of a quadratic term. Alternatively, one may make a piecewise linear fit to complex U_s–U_p relations. This latter approach has been taken by *Ahrens and Johnson* (1995a,b) in their compilation of Hugoniot data for major rocks and minerals. Data originally presented as P–U_s or P–V Hugoniots were transformed to the U_s–U_p form for these compilations. A further advantage of the U_s–U_p form is that it lends itself well to extrapolations beyond the limits of available data.

Figure 2 is a representation of a Hugoniot in the P–V plane. Strictly speaking, the Hugoniot represents only those states that are reached by a single shock from a given initial state (P_o, V_o, E_o). The Rayleigh line is the loading path, shown as a straight line connecting the initial state with the state on the Hugoniot. The energy increase on shock compression is simply the area of the right triangle ABC: (1/2) P (V_o–V). Here we neglect the P_o (one atmosphere) of equation (6). This energy increase comprises both mechanical and thermal terms. On pressure release, the mechanical portion (equivalent to the area under the release adiabat) is recovered. In general, assuming that no phase transitions have occurred, the release adiabat lies to the right of the Hugoniot because of thermal expansion. However, most rocks and their constituent minerals have low coefficients of thermal expansion. One may therefore approximate the release adiabat with the Hugoniot. Any difference between the two is usually of the same order as the uncertainty in the measurements of the Hugoniot. Indeed, this approximation is equivalent to the approximation that the free surface velocity is twice the particle velocity.

The residual energy, the cross-hatched region of Fig. 2, is often called the waste heat. If one can estimate the waste heat, one can use atmospheric-pressure heat capacity (C_p)

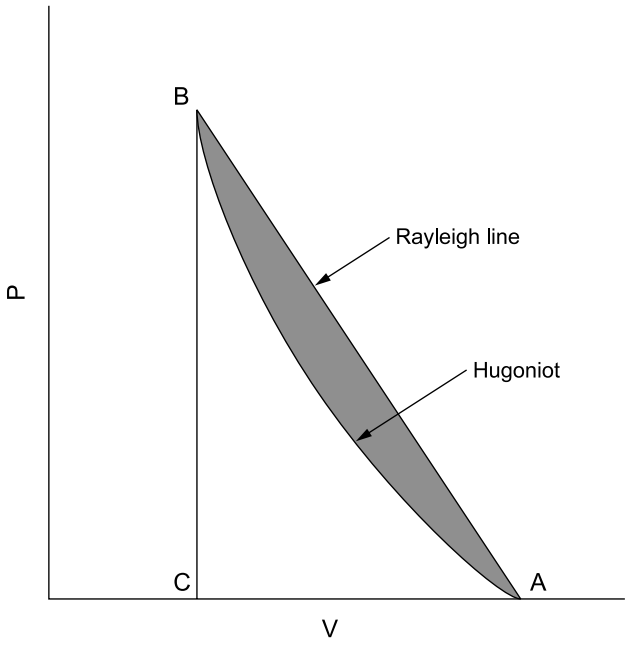

Fig. 2. Pressure-volume Hugoniot.

data on rocks and minerals to determine the postshock temperature, i.e., the temperature at the foot of the release adiabat. With a postshock temperature as a starting point one may estimate the temperature increase on adiabatic compression to the shocked state P, V. We present a simple spreadsheet technique for calculation of waste heat in Appendix A.

2.2. Porous Hugoniots

Figure 3 illustrates the typical response of a porous rock to shock compression and release. With increasing pressure, the porosity is crushed out until the pressure-volume Hugoniot becomes indistinguishable from that of an initially solid rock of the same mineralogy. In general, the porosity is not recovered on release of pressure. In the absence of release measurement data, one may use the Hugoniot of the initially solid rock to approximate the release adiabat of the initially porous rock.

Initial porosity obviously has a very large effect on waste heat. The waste heat for nonporous quartz shocked to 10 GPa is about 60 J/g. Assuming a uniform distribution of the waste heat and an initial temperature of 300 K, the postshock temperature would be ~375 K.

In contrast, the waste heat for sand, having an initial density of 1.4 g/cc (about 40% porosity) and shocked to 10 GPa is about 1740 J/g. Again assuming a uniform distribution of the waste heat and an initial temperature of 300 K, the postshock temperature would be about 1820 K. We know that the initial distribution of waste heat is highly nonuniform, as shown by Baer's calculations and Kieffer's observations. We also know that the pressure history in the sand was chaotic on a nanosecond timescale. Micrometer-sized regions of the sand could have experienced nanosecond-duration spikes of 50–100 GPa. However, the only number we can reliably calculate is the continuum value of 10 GPa to which the chaotic pressure distribution equilibrates within less than a microsecond (for millimeter-sized grains). For millimeter-scale thermal inhomogeneities, the equilibration time would be on the order of seconds. Shock temperature calculations for initially porous materials are valid only for very long-duration shocks.

The waste heat estimate is an approximation of the entropy increase over the cycle of compression and release. Strictly speaking, the waste heat method of estimating postshock temperature applies to the one-dimensional shock propagation geometry of Fig. 1. In most natural impacts, heating due to plastic strain in divergent flow and in tension may add substantially to the postshock temperature. Also note that localized hot spots or bands may form during shock deformation of nonporous homogeneous materials. The phenomenon of adiabatic shear, first observed in metals by *Zener and Hollomon* (1944), may account for some of the melt veins observed in meteorites.

In current models of the early solar system, mineral grains condense as the temperature of the solar nebula decreases. These mineral grains then aggregate, eventually forming larger bodies. One may infer that collisions among porous bodies aid in their compaction and lithification. For 1.4 g/cc sand, 10 GPa corresponds to a particle velocity of ~2 km/s. Two bodies of that porosity would have to collide at a relative velocity of ~4 km/s to achieve a continuum pressure of 10 GPa at the point of impact. We emphasize that the peak pressure is obtained at the point of impact; shocks attenuate rapidly in porous materials because the release wave velocities in compressed material are much higher than the shock velocities in the porous material. *Rubin* (2005) has hypothesized that shock compression of porous material provided a significant heat source for meteorite parent bodies in the early solar system. Rubin suggests that it may even be necessary to invoke shock compression as a heat source. Should this be the case, one could perform a series

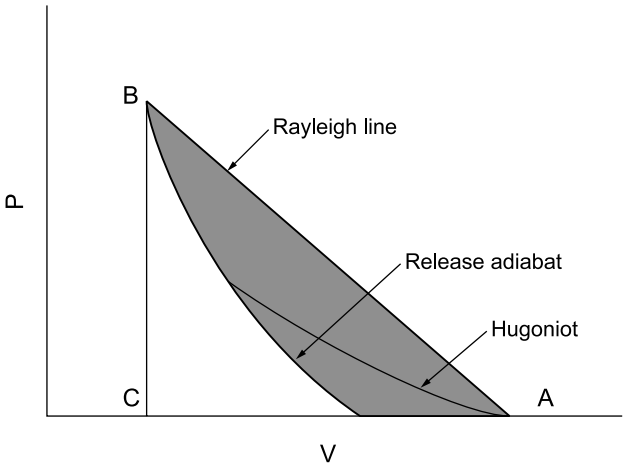

Fig. 3. Pressure-volume response of a porous material.

of hydrocode calculations of impacts to test models of the size distribution and collisional probabilities (including relative collision velocities) of porous parent bodies in the early solar system.

2.3. Phase Transitions on the Hugoniot

In an earlier era, shock wave workers were hard pressed to account for the apparent rapidity of shock-induced phase transitions, e.g., of graphite to diamond *(DeCarli and Jamieson,* 1961). *Alder*'s (1963) arguments were typical of those ascribing "special" characteristics to shock compression. Subsequent work on shock synthesis of diamond indicated that polycrystalline cubic diamond could form via an ordinary nucleation and growth mechanism in hotspots created by shock interactions (jetting) around pores (*DeCarli,* 1979, 1995). Conditions for shock synthesis of diamond were predictable on the basis of static high-pressure experiments (*Bundy and Kasper,* 1967) on the direct (uncatalyzed) synthesis of diamond. Bundy and Kasper observed that conditions for direct diamond synthesis were sensitive to the crystalline perfection of the carbon starting material. Poorly crystalline graphitic carbons required transient (microsecond-duration) temperatures above ~3000 K and pressures above ~15 GPa. The resultant diamond is cubic, polycrystalline, and optically isotropic. If the starting material were a well-ordered natural graphite, transformation occurred at lower transient temperatures in the range of 1300 K to 2000 K. The resulting diamond is a polycrystalline optically anisotropic mixture of cubic and hexagonal (lonsdaleite) diamond. The hexagonal phase has a preferred orientation, (100) parallel to (001) graphite. This latter form of direct-transition diamond has been made in laboratory shock experiments and it is the form commonly found in both meteorites and in impact craters (*DeCarli et al.,* 2002a). To date, we have found no evidence to contradict our working hypothesis that conditions for shock-induced phase transitions can be generally predicted on the basis of static high-pressure data. In other words, the physics of phase transformations during shock are the same as in static experiments. However, one must be aware that the detailed correlations between static high-pressure observations and observations on shocked minerals will necessarily be imperfect because of differences in detailed pressure-temperature-time histories between shock and static loading and unloading paths.

Numerous Hugoniot measurements on rocks and minerals have been interpreted in terms of phase transitions to denser phases. However, the evidence for phase transitions is often circumstantial. For example, Hugoniot data on pyroxenes and olivines indicate that they compress to densities appropriate to high-pressure phases (*Ahrens and Gaffney,* 1971; *Ahrens et al.,* 1971). However, their measured release adiabats are indistinguishable from their Hugoniots, within the limits of measurement error. Furthermore, there is no evidence from shock-recovery experiments, up to 80 GPa, that phase transformations of olivines and pyroxenes have occurred (*Jeanloz,* 1980). There are localized occurrences of high-pressure phases of olivine and pyroxene in many meteorites, as will be discussed in detail later in this paper. The high-pressure phases are invariably found in regions that appear to have been subjected to localized high temperatures, either in or adjacent to the so-called melt veins of meteorites. The shock behavior of olivines and pyroxenes thus appears consistent with static high-pressure studies that show their phase transformations to be very sluggish at modest temperature.

In contrast, there is excellent evidence that quartz and feldspars undergo phase transitions under shock compression. At shock pressures above about 30 GPa, these minerals have volumes appropriate to more densely packed phases. Some workers interpret the Hugoniot data in terms of phase transitions to crystalline phases, e.g., stishovite or hollandite. This interpretation is contradicted by *Panero et al.* (2003), who observe that the high-pressure Hugoniot data on quartz indicate somewhat lower densities at pressure than do static high-pressure measurements on stishovite. Measured Hugoniot release adiabats indicate that the densely packed phases persist on release down to a pressure of about 7 GPa. Upon further release to zero pressure, the volume increases to a final state about 20% greater than the initial volume. These release data support the view that the inferred Hugoniot transitions are primarily to close-packed disordered phases that invert to low-pressure disordered phases (i.e., diaplectic glass) on release of pressure. This view is supported by shock-recovery experiments in which the bulk of the sample is recovered as diaplectic glass (*DeCarli and Jamieson,* 1959; *Milton and DeCarli,* 1963). Again, the shock wave data are consistent with the results of static high-pressure experiments. In room-temperature static experiments at pressures above about 12 GPa, quartz and feldspars transform to dense amorphous phases that invert to low-density amorphous phases on release of pressure (*Hemley et al.,* 1988; *Williams and Jeanloz,* 1989). Hugoniot and release adiabat data on albite (*Ahrens and Gregson,* 1964; *Ahrens and Rosenberg,* 1968) are shown in Fig. 4.

Release paths from pressures above about 35 GPa are very steep, appropriate for complete transformation to a close-packed disordered structure. Release paths from pressures below about 20 GPa are indistinguishable from the Hugoniot and imply no significant transformation. Measured release paths from intermediate pressures, e.g., 28 GPa, are indicative of partial transformation and lie between the extremes illustrated in Fig. 4. Release adiabats and Hugoniots are measured in microsecond-duration experiments. The fact that the Hugoniot transition pressure is higher than observed in static experiments implies that kinetic factors are important. Kinetic factors could account for the observation of complete transformation of feldspars in meteorites that appear to have been subjected to modest pressures (21–25 GPa) over a long duration (0.01–1 s) (e.g., *Xie et al.,* 2005).

As noted earlier, the postshock temperature may be estimated by determination of the waste heat, the difference

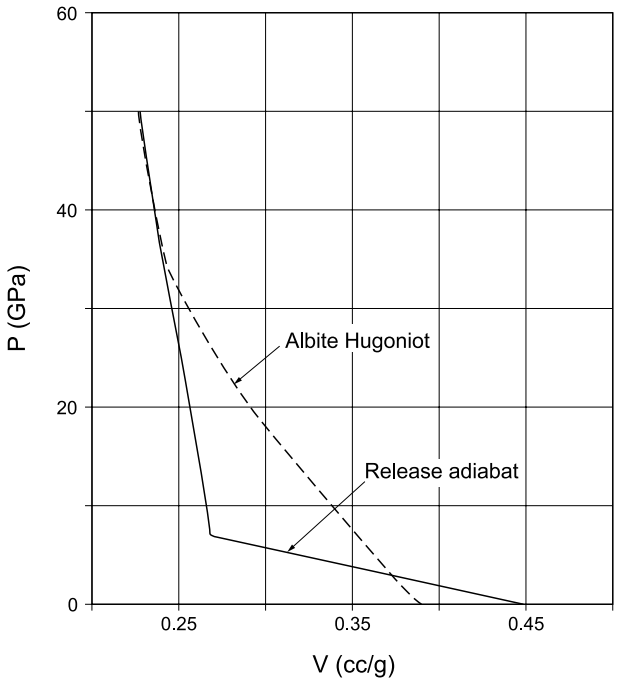

Fig. 4. Hugoniot and release adiabat data for albite (*Ahrens and Rosenberg,* 1968).

between the total energy increase on shock compression, and the mechanical energy recovered on adiabatic release. Phase transitions of the type illustrated in Fig. 4 can have a very large effect on the waste heat. If one uses the Hugoniot to approximate the release adiabat, the calculated waste heat on release for 35 GPa is ~320 J/g, corresponding to a postshock temperature of ~600 K (assuming an initial T of 300 K). If one uses the release adiabat shown in Fig. 3, the calculated waste heat on release is ~1250 J/g, corresponding to a partial melt at 1373 K. Simple postshock temperature calculations thus indicate that diaplectic glass formation, in both quartz and feldspar, is limited to a relatively narrow pressure range.

2.4. Shock Reflections and Loading-Path Effects

Shock interactions such as rarefactions or reflections take place at interfaces between materials of different shock impedance. To illustrate the effects of shock interactions on loading path, we assume the simple one-dimensional geometry illustrated in Fig. 5. Using materials for which we have Hugoniot data, we choose an albite inclusion in an iron meteorite. This example may not be particularly relevant to an actual iron meteorite, but it is similar to the high shock impedance container geometry used in many shock-recovery experiments (*Milton and DeCarli,* 1963).

The inclusion has infinite lateral extent but finite thickness, and the direction of shock propagation is normal to the plane of the inclusion. We assume a flat-topped shock pressure pulse in the iron having an amplitude of 50 GPa. Since albite has a much lower shock impedance than Fe-Ni, the initial shock transmitted into the albite will be less than 50 GPa; pressure equilibration will be achieved by a sequence of shock reflections. The detailed pressure history of the inclusion is calculated through the use of Hugoniots in the P–U_p plane, as shown in Fig. 6.

The albite Hugoniot lies well below the iron Hugoniot. When the shock arrives at the iron-silicate interface, the shock pressure on both sides of the interface must become equal and the particle velocities on both sides must also become equal, in accordance with the Hugoniots and release adiabats of both materials. As shown in Fig. 6, the initial state, 24.4 GPa, is achieved at the intersection of the iron release adiabat originating from 50 GPa with the Hugoniot of the silicate. The result is a transmitted shock into the silicate and a release wave moving backward into the iron. When the shock reaches the downstream silicate-iron interface, pressures and particle velocities must again be matched. The reflected shock state, 38.9 GPa, corresponds to the intersection of the reflected shock Hugoniot of the albite with the iron Hugoniot. A pressure of 46.2 GPa is reached via a second shock reflection. After several more reflections, the pressure in the silicate closely approaches the initial 50 GPa in the iron. The equilibration time is simply the sum of the shock transit times through the inclusion thickness. Albite shock velocities over the pressure regime of interest are 5–7 km/s; a 1-mm-thick inclusion would "ring up" to pressure equilibrium in less than a microsecond.

The thermodynamic final state achieved in the silicate via successive reflections is not the same state that would be achieved in a single shock, as illustrated in Fig. 7. The total energy increase is the sum of the areas under each Rayleigh line. For the reflected shock case illustrated above, the waste heat on release from 50 GPa is ~1040 J/g, equivalent to a postshock temperature of 1220 K (for an initial temperature of 300 K). For albite shocked in one step to 50 GPa, the waste heat on release is ~2060 J/g, equivalent to a liquid at a temperature of 1770 K. Although the same peak pressures may be achieved via single shock and re-

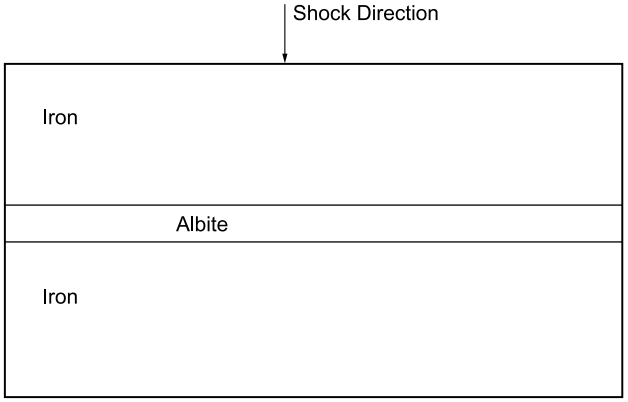

Fig. 5. Representation of a planar albite inclusion in an iron meteorite.

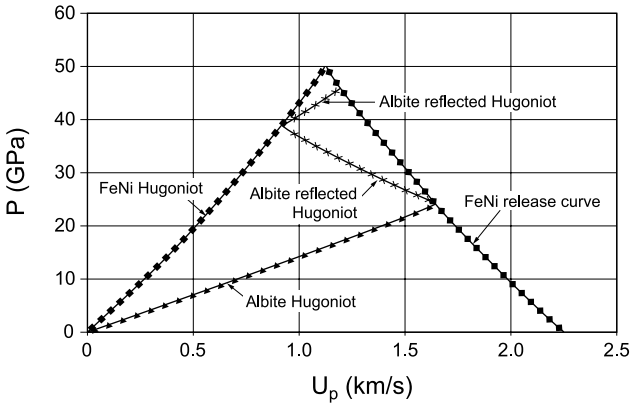

Fig. 6. Pressure equilibration via reflected shocks.

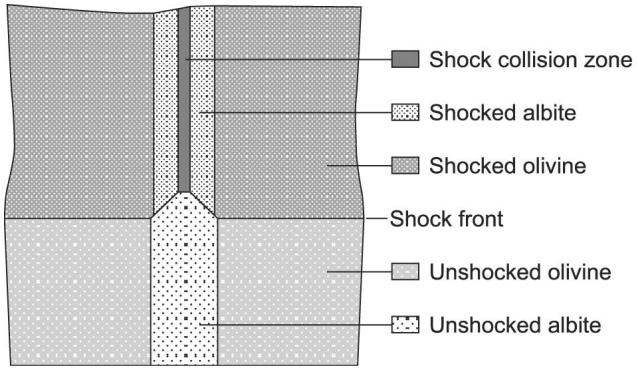

Fig. 8. Shock collision example.

flected shock loading paths, calculated waste heats may differ by a factor of 2 or more.

2.5. Shock Collisions

In the continuum model of plane shock propagation in a polymineralic rock, the Hugoniot represents averaged values of shock velocity, particle velocity, and pressure. On the scale of these averaged values the shock front is planar. On the scale of the grain size (or smaller), the shock front may be very irregular because of shock velocity differences among the different minerals. Analogous with the refraction of light, the shock front may be refracted at interfaces between different minerals. Refracted shock fronts may collide, producing localized (micrometer-scale) pressure spikes (nanoseconds-duration) in the low-impedance mineral that greatly exceed the pressure in the high-impedance minerals. We present a simple example in Fig. 8.

Figure 8 represents a thin plate of albite between two forsterite grains. This is similar in appearance to Fig. 5, except that the shock is traveling parallel to the plane of the low-impedance inclusion. For a pressure of 30 GPa, the shock velocity is 7.86 km/s in the forsterite. The shock velocity in albite at 30 GPa is only 5.84 km/s. As a consequence, the shock fronts are refracted at the forsterite-albite interfaces. The refracted shock fronts collide at the albite midplane, and the collision region (of finite width) is forced to propagate at the 7.86 km/s velocity of the shock in the forsterite. From the Hugoniot of albite, a shock velocity of 7.86 km/s corresponds to a pressure of 70 GPa. This high-pressure, high-temperature albite in the central region will "ring down" to 30 GPa. The calculated waste heat of 3300 J/g corresponds to a postshock temperature of about 2700 K. Assuming a Grüneisen parameter of 1.5, the calculated shock temperature at the continuum pressure of 30 GPa would be ~3280 K, more than sufficient for melting on the Hugoniot. The albite near the interface with the forsterite will "ring up" to 30 GPa. Assuming negligible phase transformation, the calculated shock temperature is ~550 K; assuming complete phase transformation, the calculated shock temperature is ~1300 K.

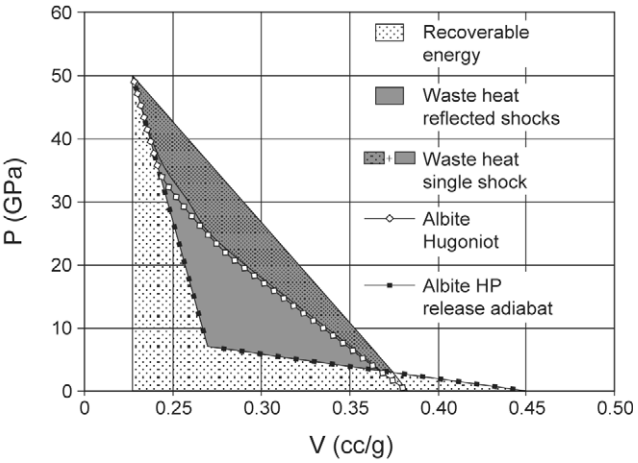

Fig. 7. Comparison of waste heat in albite for single vs. reflected shock compression to 50 GPa.

2.6. Further Comments on Shock Wave Heterogeneity

The simple examples we have presented are intended to provide an introduction to the complexities of shock wave propagation in a real three-dimensional polymineralic rock. However, the greatest source of localized pressure and temperature heterogeneity is the interaction of shock waves with cracks and pores. Kieffer's inferences of shock interaction effects in shocked Coconino sandstone were informed by knowledge of the porosity of the unshocked material (*Kieffer,* 1971; *Kieffer et al.,* 1976). Unfortunately, we do not have direct information on the nature of the porosity in a given meteorite prior to the shock event that produced the effects of interest. We are particularly interested in melt-vein-producing shock events. Shock collisions due to grain-scale heterogeneities as described above could form narrow veins in low-impedance minerals like feldspar and graphite, but

cannot account for veins in olivine and pyroxene. Adiabatic shear might account for narrow planar melt veins (*Schmitt and Ahrens,* 1983), but many melt veins and pockets are neither planar nor narrow. Furthermore, adiabatic shear is often correlated with the flow divergence during pressure release (*Nestorenko,* 2001). Shock wave interaction along cracks and pores is one explanation that could account for the melt veins and pockets observed in many highly shocked meteorites. This explanation satisfies simple energy balance estimates. For a nonporous chondrite with the composition of Tenham, we calculate a waste heat of ~80 J/g (about 100° above its preshock temperature) on release from a shock pressure of 25 GPa. If the initial porosity were ~0.07, a typical value for chondrites (*Consolmagno and Britt,* 1998), the waste heat on release from 25 GPa would be ~320 J/g. Assuming the porosity is in the form of cracks, one could predict that the "excess" waste heat of 240 J/g (320–80) would be deposited in the vicinity of the cracks. The energy required to melt forsterite, starting from an initial temperature of 300 K, is about 3000 J/g. Thus 240 J/g would account for a melt vein fraction of about 0.08 in Tenham, consistent with our observations on Tenham (*Xie et al.,* 2005).

Although the melt is the result of a transient and localized high pressure, the melt persists long after the pressure spike has rung down to the continuum pressure. Any observations on the vein should be relevant to the continuum pressure and its decay as the melt solidified and thermally equilibrated with the surrounding cooler material. For example, it has been shown that the effect of shocking a granular sample in a gaseous environment can be to trap gas in the shock compacted aggregate (*Fredriksson and DeCarli,* 1964; *Pepin et al.,* 1964; *Wiens and Pepin,* 1988). In retrospect, one can explain these results as the expected consequence of ordinary diffusion in a thermally heterogeneous high-pressure environment. The high-pressure gas would diffuse into the localized hot (even molten) regions, which are then quenched by conduction. One might have anticipated that melt veins in martian meteorites could contain copious amounts of martian atmosphere (*Bogard and Johnson,* 1983). In contrast, a meteorite that cools from its postshock temperature in a low-pressure environment would be expected to lose some of its radiogenic gas (*Davis,* 1977).

We pointed out earlier that waste heat (a proxy for postshock temperature) is much lower for reflected shock loading (ringing up to continuum pressure) in comparison with single shock loading to the same continuum pressure. Shock-recovery experiments have been performed on preheated samples in an attempt to compensate for the waste heat difference between single shock and reflected shock experiments. However, the preheating does not compensate for the fact that localized pressure and temperature heterogeneities are also substantially reduced in reflected shock loading (*DeCarli et al.,* 2002a). Shock interactions around cracks and pores can occur only during passage of the initial shock because the subsequent shock reflections pass through compressed nonporous material.

Up to this point, we have discussed shock propagation through materials that are heterogeneous on a millimeter scale. One must also consider the possibility of larger-scale heterogeneities in a meteorite parent body. For example, consider a material having open cracks with a spacing of about 10 cm. The initial chaotic period of pressure equilibration to the continuum value could span as much as 100 μs. Approximate analyses indicate that shock collisions within these 10-cm blocks and shear localization now become viable mechanisms for production of melt veins within the blocks. One would also predict that the former open cracks would become large melt veins. In principle, one could refine these approximate analyses with detailed shock propagation calculations for a range of possible crack spacings and crack openings.

It is important to recognize that interpretations of shock effects in meteorites are often influenced by unstated assumptions concerning the overall structure of a parent body and the detailed properties of the region of the parent body from which a meteorite originated. We prefer simple models because they permit quantitative evaluation of shock propagation and heat flow effects. One must admit, however, that quantitative efforts may be irrelevant if the model differs too much from reality.

2.7. Limitations of Hugoniot Measurements and Shock-Recovery Experiments

The major limitation of Hugoniot measurements is that they are made in relatively short-duration (<10 μs) experiments. Many shock wave workers have speculated that kinetic effects on phase transitions might be important in millisecond- or longer-duration shock events, but it is either prohibitively expensive or impossible to perform long-duration shock compression measurements in the appropriate stress range for most mineral phase transitions of interest. Our working hypothesis is that the results of very long-duration shock events will be consistent with the results of static high-pressure experiments. *DeCarli et al.* (2002b) have recently interpreted Meteor Crater shocked Coconino sandstone mineralogy in terms of evidence for kinetic effects, but alternative explanations have not been ruled out.

Shock-recovery experiments have duplicated many, but not all, of the metamorphic features observed in meteorites. However, the range of shock conditions (loading paths, peak pressure, peak pressure duration, unloading paths, etc.) accessible in laboratory shock-recovery experiments is sharply limited in comparison with natural events. As implied by our discussion of the phase transitions in quartz and feldspars, we question the relevance to meteorite studies of the pressure calibration scales developed in shock-recovery experiments. Furthermore, many experimental studies report their results in terms of a single parameter, shock pressure, and do not provide enough detailed information on the experimental design to permit independent assessment of other relevant factors such as loading and unloading paths.

However, one may point to a recent paper by *Tomeoka et al.* (1999) that does provide detailed information on the experiment, including impact velocity, flyer plate material and dimensions, sample container material, sample mate-

rial and dimensions, and the assumptions of the calculations that were made. They properly interpreted their reflected shock experimental data as equivalent to much-lower-pressure natural events. The Murchison Hugoniot (*Anderson and Ahrens,* 1998) that they used to interpret their results understates the initial porosity of the meteorite. As a consequence, their calculated waste heat is too low, 600 J/g vs. our calculation of 900 J/g, for the sample loaded to 48.8 GPa via reflected shocks. However, their conclusion is unchanged. Reflected shock loading to 48.8 GPa is equivalent, in terms of waste heat, to single shock loading to ~17 GPa. *Tomeoka et al.* (1999) also describe the deformation observed in their recovered samples. In our opinion, this deformation is attributable to the details of pressure release, specific to the conditions of the experiment and not necessarily relevant to a natural event. We will not attempt to estimate the additional heating ascribable to deformation in their experiments.

Experiments reported by *Huffman et al.* (1993) provide a measure of deformational heating. They observed bulk melting in shock-recovery experiments at 5 GPa on samples of Westerly granite preheated to 750°C in high-impedance stainless steel containers. We calculate that a temperature increase of only 20° could be attributed to the waste heat increase on compression and release. However, *Huffman et al.* (1993) also report that some of their samples were reduced in thickness by as much as 50%. One may infer that the observed melting may be attributable to the additional heating from plastic deformation.

The starting point for interpretation of shock effects in meteorites is in detailed observations on the meteorites. To interpret these observations, one uses all the relevant information available, including Hugoniot measurements, results of shock-recovery experiments, and results of static high-pressure studies.

As shown above, it may be useful to reinterpret some experimental results on the basis of simple shock wave calculations. All interpretations should be tested for consistency with existing knowledge of heat flow, diffusion, and phase transformation kinetics, *inter alia*. We have tried to emphasize the importance of details, e.g., presence of pores and cracks and grains of differing shock impedance, that influence shock wave propagation and loading paths. It is also useful to remember, when examining a two-dimensional slice at high resolution, that shock waves propagate in three dimensions. Given one's ignorance of relevant details that are either unknown or out of the plane of observation, one must be willing to admit the possibility of alternate interpretations.

2.8. Shock Metamorphism and Shock Classification in Meteorites

The metamorphic effects seen in shocked meteorites can be described in terms of either deformation or transformation or some combination of the two. Shock effects in meteorites and terrestrial rocks have been discussed at length in other papers (*Chao,* 1967, 1968; *Heymann,* 1967; *Kieffer,* 1971; *Scott et al.,* 1992; *Stöffler,* 1972, 1974; *Stöffler et al.,* 1991; *Ashworth,* 1985; *Bischoff and Stöffler,* 1992; *Leroux,* 2001; and many more) and so only a subset of shock effects will be discussed here.

Deformational effects include fracturing, plastic deformation, twinning, and mosaicism within constituent minerals. Planar shock features, generally referred to as planar deformation features (PDFs) (*Goltrant et al.,* 1991, 1992; *Langenhorst et al.,* 1995), have been attributed to deformational processes, but they have also been shown to contain transformed material, either diaplectic glass or high-pressure phases (*Goltrant et al.,* 1991; *Bowden,* 2002). The term planar deformation feature is therefore misleading because it neglects the transformation component. We will not discuss shock-induced deformation effects in this paper.

Transformational effects seen in shocked meteorites include shock melting, which commonly results in localized melt veins and pockets, transformation of minerals to high-pressure polymorphs, formation of diaplectic glass, and recrystallization of highly deformed material. The high-pressure minerals that occur in shocked meteorites form by either crystallization of silicate liquids in melt veins and pockets, or by solid-state transformation of the constituent minerals in the meteorite (*Chen et al.,* 1996). Solid-state phase transformations can provide important constraints on shock conditions of a meteorite, but transformation pressures are difficult to calibrate accurately because of kinetic effects and the heterogeneous nature of the initial transient shock pressures. Crystallization of chondritic melt provides an alternative means of constraining the crystallization pressure, which can be related to the shock pressure of the sample. In this part of the paper we will discuss high-pressure minerals in shocked meteorites and the constraints that they can provide for the interpretation of shock pressure and duration.

The shock effects in meteorites have been classified and calibrated to shock pressure by many previous workers (*Heymann,* 1967; *Carter et al.,* 1968; *Van Schmus and Ribbe,* 1968; *Taylor and Heymann,* 1969; *Dodd and Jarosewich,* 1979; *Sears and Dodd,* 1988; *Stöffler et al.,* 1988, 1991; *Schmitt,* 2000; *Leroux,* 2001). *Stöffler et al.* (1991) made a significant revision of previous classification systems by concentrating on petrographically observable shock effects in olivine and plagioclase. Incorporating a large database of experimental shock results, *Stöffler et al.* (1991) classified the shock effects in ordinary chondrites as six distinct shock stages, S1–S6. An advantage of the Stöffler et al. system is that the shock features used are those of olivine and plagioclase, which are common in ordinary chondrites and many achondrites. The characteristic shock features are easy to observe with a petrographic microscope and therefore the classification system has become readily used in the shock classification of meteorites. The characteristic shock effects are S1 (unshocked), sharp optical extinction; S2 (very weakly shocked), undulatory extinction in olivine; S3 (weakly shocked), planar fractures in olivine; S4 (moderately shocked), mosaicism in olivine; S5 (strongly shocked), maskelynite formation and planar deformation features in olivine; S6 (very strongly shocked), recrystallization of oli-

vine that can be combined with high-pressure phase transitions such as the formation of ringwoodite. S6 features are described as "restricted to regions adjacent to melted portions of the sample which is otherwise only strongly shocked." Stöffler et al. interpret the S6 features to represent local pressure and temperature "excursions" or spikes that develop as a result of local variations in shock impedance. In this interpretation, the S6 shock effects would have to form under transient pressure spikes before they were rung down to the continuum shock pressure corresponding to S5 conditions. *Spray* (1999) proposed an alternative mechanism of cavitation (bubble implosion) within shock melt to produce local pressure spikes during pressure release that could transform olivine to ringwoodite in and along melt veins. In both models, high-pressure phase transitions are caused by local pressure spikes that exceed the equilibrated peak pressure of the rock. In the *Stöffler et al.* (1991) model, the pressure spikes would be early in the shock event, whereas in the *Spray* (1999) model, the pressure spikes would occur during pressure release. One objection to the Spray model is that the melt veins of many meteorites contain high-pressure phases that must have crystallized from the melt as it cooled via conduction. Spray's model would predict the presence of low-pressure phases in the melt veins. The problem with *Stöffler et al.*'s (1991) interpretation of S6 "pressure-temperature excursions" is that it overemphasizes the role of pressure (*Xie and Sharp,* 2004). As discussed in the background section, the pressure heterogeneities generated by shock wave interactions ring down to the continuum shock pressure within about 1 μs for a material with millimeter-scale impedance heterogeneities. The phase transformations that define S6 shock effects require high-pressure conditions for much longer than 1 μs (*Ohtani et al.,* 2004; *Chen et al.,* 2004b; *Beck et al.,* 2005; *Xie et al.,* 2005).

Although the shock stages of *Stöffler et al.* (1991) correctly reflect the sequence of increasingly more metamorphosed material, there are several reasons why the corresponding pressure calibration provides shock pressure estimates that are too high. The pressure calibration of Stöffler et al., which is based on shock-recovery experiments, defines the S1/S2, S2/S3, S3/S4, S4/S5, and S5/S6 transitions as <5, 5–10, 15–20, 30–35, and 45–55 GPa, respectively, with S6 conditions including pressures up to 90 GPa. *Schmitt* (2000) points out that although ordinary chondrites are porous, the samples used in most shock-recovery experiments, which commonly include single crystals and igneous rock fragments, are not porous. As discussed in the section on porous Hugoniots, the internal energy increase of shock compression is much higher for initially porous materials. Recognizing that shock-recovery experiments on nonporous samples result in relatively low shock temperatures, Schmitt did shock-recovery experiments at elevated starting temperatures (920 K) as well as at low temperature (293 K) to investigate the temperature effect on shock metamorphism pressures for the H chondrite Kernouvé. The importance of kinetics in shock metamorphism is illustrated by the fact that maskelynite formation occurred at 20–25 GPa in the preheated experiments compared to 25–30 GPa in the low-temperature samples and 30–35 GPa in the *Stöffler et al.* (1991) study. These and other high-temperature shock experiments demonstrate that shock metamorphic effects are temperature dependent as well as pressure dependent and that one cannot accurately calibrate the shock pressures without considering kinetic effects. Because kinetic effects are important, one may further question the relevance of microsecond-duration shock-recovery experiments to much-longer-duration natural shock events.

In addition to the porosity problem, shock-recovery experiments done in high-shock-impedance sample containers result in high shock pressures and relatively low shock temperatures (*Bowden,* 2002). As discussed in the section on shock reflections and loading path effects, samples in high impedance containers reach peak (continuum) pressure via a series of shock reflections, with the result that shock and postshock temperatures are substantially lower than for a sample loaded via a single shock to the same peak pressure (*Bowden,* 2002; *DeCarli et al.,* 2002b). For example, *Bowden* (2002), who shocked quartz sand in containers of various shock impedances, produced multiple intersecting planar features at 8 GPa in impedance-matched polyethylene containers and at 19 GPa in high-impedance stainless steel containers. Since most of the shock-recovery data used in the *Stöffler et al.* (1991) calibration were from experiments in high-impedance containers, the calibrated pressures of thermally activated shock effects, such as phase transformations, are likely to be too high.

2.9. High-Pressure Minerals in Meteorites

High-pressure minerals are common in and around melt veins in highly shocked meteorites (*Binns et al.,* 1969; *Binns,* 1970; *Smith and Mason,* 1970; *Putnis and Price,* 1979; *Price et al.,* 1983; *Langenhorst et al.,* 1995; *Chen et al.,* 1996; *Sharp et al.,* 1997; *Tomioka and Fujino,* 1997; *Langenhorst and Poirier,* 2000b; *Gillet et al.,* 2000; and others). The discovery of ringwoodite, the spinel-structured polymorph of olivine, in Tenham (*Binns et al.,* 1969) provided proof that Tenham had experienced very high shock pressures. Ringwoodite had already been observed in the Coorara chondrite by *Mason et al.* (1968), but it was misidentified as garnet based on X-ray diffraction data from the majorite garnet in the sample. *Smith and Mason* (1970) clarified the mistake when they published the discovery of majorite garnet in Coorara. The majorite that they describe occurred in a fine-grained mixture of garnet, Fe-oxide, and Fe, which must have been crystallized chondritic melt such as that described by *Chen et al.* (1996). The fact that these garnets had higher concentrations of Na, Al, and Cr than the orthopyroxenes in the sample confirms that they crystallized from a melt. In the same paper, *Smith and Mason* (1970) describe an isotropic phase with an orthopyroxene composition that they speculated was also majorite. It was clear from this early work that Tenham and Coorara had experienced high

pressures. Although the significance may not have been realized at the time, it is clear from this work that ringwoodite and majorite were only observed in close association with melt veins. *Putnis and Price* (1979) used transmission electron microscopy (TEM) to characterize the microstructures of ringwoodite in Tenham and subsequently discovered the β-spinel polymorph of olivine, which they later named wadsleyite. Although the high-pressure minerals were used to interpret shock effects in meteorites (*Price et al.,* 1979, 1983) much of the subsequent work on naturally occurring ringwoodite and wadsleyite in meteorites was focused on defects and transformation mechanisms that might be important in Earth's mantle (*Price et al.,* 1982; *Madon and Poirier,* 1983; *Price,* 1983). More recent work concerning high-pressure minerals in meteorites (*Langenhorst et al.,* 1995; *Chen et al.,* 1996, 2004b; *Sharp et al.,* 1997, 1999; *Tomioka and Fujino,* 1997; *El Goresy et al.,* 2000; *Gillet et al.,* 2000; *Tomioka et al.,* 2000; *Xie et al.,* 2005; and others) have returned the focus back to interpreting shock conditions and durations.

Numerous other high-pressure minerals have been found in shocked meteorites since the time of ringwoodite and majorite discoveries. In nearly all cases, the high-pressure polymorphs occur within shock melt or adjacent to it. Mori appears to have been the first to discover a number of high-pressure phases including magnesiowüstite in melt veins (*Mori and Takeda,* 1985), plagioclase with the hollandite structure, and a glassy $MgSiO_3$-rich material that was inferred to be $MgSiO_3$-perovskite that was vitrified after pressure release (*Mori,* 1994). Magnesiowüstite was rediscovered by *Chen et al.* (1996), who realized that it crystallized along with majorite-pyrope garnet from chondritic melt in Sixiangkou. *Chen et al.* (1996) pointed out that one could use the mineral assemblages that crystallize from chondritic melt to estimate melt-vein crystallization pressure. Akimotoite, the ilmenite-structured polymorph of $MgSiO_3$, was discovered almost simultaneously by *Sharp et al.* (1997) and *Tomioka and Fujino* (1997) in Acfer 040 and Tenham, respectively. In Acfer 040, akimotoite crystallized directly from the melt (*Sharp et al.,* 1997), whereas in Tenham, the akimotoite formed from enstatite by a solid-state phase transition (*Tomioka and Fujino,* 1997). In both of these studies, a form of silicate perovskite was also described. In Tenham, the silicate perovskite, like the akimotoite, formed directly from enstatite by a solid-state mechanism (*Tomioka and Fujino,* 1997). However, in Acfer 040 equant domains of glass surrounded by akimotite and ringwoodite were interpreted as silicate perovskite that had crystallized from the melt and subsequently vitrified after pressure release (*Sharp et al.,* 1997). Similar material had already been found by *Mori* (1994) and has been subsequently found in Zagami (*Langenhorst and Porier,* 2000a) and in Tenham (*Xie et al.,* 2005). Plagioclase with the hollandite structure was rediscovered in Sixiangkou (*Gillet et al.,* 2000) and in Tenham (*Tomioka et al.,* 2000). This material occurs as polycrystalline aggregates with crystals that are tens of nanometers in size. Similar hollandite has been found in Umbarger (*Xie and Sharp,* 2004). Two new poststishovite polymorphs of silica were discovered in the martian meteorite Shergotty (*Sharp et al.,* 1999; *El Goresy et al.,* 2000). These polymorphs have an orthorhombic α-PbO_2 structure and a monoclinic ZrO_2-like structure, respectively, that are both slightly denser than stishovite. *Chen et al.* (2003) also discovered two high-pressure polymorphs of chromite in the Suizhou L6 chondrite.

Maskelynite is a form of amorphous plagioclase feldspar that was first described by *Tschermak* (1872). It was demonstrated to be a diaplectic glass formed by shock metamorphism when it was synthesized in a shock-recovery experiment (*Milton and DeCarli,* 1963). As discussed in the section on shock-induced transformations on the Hugoniot, the transformations of feldspars to maskelynite and crystalline silica to diaplectic quartz appear to take place on compression. Although the high temperatures associated with melt veins are not needed for the formation of maskelynite, higher temperatures do enhance the transformation around shock-melt veins and pockets. The formation of maskelynite is directly linked to the formation of PDFs in plagioclase, which represents partially transformed material. In the melt regions of highly shocked samples, plagioclase has been described as normal glass, which was interpreted to have melted during shock (*Stöffler et al.,* 1991). *Chen and El Goresy* (2000) have also demonstrated that what appears to be maskelynite can actually be melted plagioclase that quenched to glass. However, in very highly shocked samples the glassy plagioclase that occurs within or adjacent to shock melt can be nanocrystalline material with the hollandite structure. This has been documented by Raman spectroscopy in Sixiangkou (*Gillet et al.,* 2000) and by TEM in Tenham (*Tomioka et al.,* 2000; *Xie and Sharp,* 2003; *Xie et al.,* 2005) and by TEM in Umbarger (*Xie and Sharp,* 2004).

2.10. Mechanisms of Solid-State Transformations

The mechanisms by which low-pressure minerals transform into their high-pressure polymorphs during shock are important for understanding the kinetics of shock effects. Here we review the mechanisms of solid-state polymorphic reactions in general and then use the microstructures of high-pressure minerals in chondrites to infer the transformation mechanisms that occur during shock metamorphism.

The transformation of minerals to their high-pressure polymorphs can be described as displacive, reconstructive, or martensitic-like mechanisms. In a displacive phase transition, the structural difference between the polymorphs is small and can generally be described as minor displacements of the atom positions, resulting in a symmetry change that does not require breaking of bonds. These transitions are nonquenchable in that the high-pressure polymorph will spontaneously transform to the low-pressure polymorph upon pressure release. Such a displacive transition occurs between the high-pressure form of clinoenstatite (high-

clinoenstatite with space group C2/c), which transforms to low-clinoenstatite ($P2_1/c$) upon decompression at about 10 GPa for $MgSiO_3$ (*Angel et al.,* 1992; *Hugh-Jones et al.,* 1996).

Reconstructive phase transitions involve a much more substantial change in crystal structure that involves the breaking of bonds and the formation of new bonds. These transitions have much higher activation energies, generally require high temperatures, and occur by nucleation and growth. Nucleation can occur homogeneously throughout the crystal of the parent phase or it can occur heterogeneously at defect sites or grain boundaries of the parent phase. In some cases, the new structure has a crystallographic relationship and coherent grain boundary relations with the initial structure. Phase transitions that involve a common interface and generally have only two crystallographic directions in common are called epitaxial, whereas transitions that involve a common sublattice and a three-dimensional crystallographic orientation relationship are known as topotaxial. If the new phase has a chemical composition that is different from that of the initial phase, then growth of the new phase will require diffusion of atoms to and away from the growing crystal. The rate of growth in this case is known as diffusion controlled because the rate is limited by rates of long-range diffusion. An example of nucleation with diffusion-controlled growth is the equilibrium transformation of $(Mg,Fe)_2SiO_4$ olivine to wadsleyite. In this case, the equilibrium composition of the wadsleyite is more Fe_2SiO_4-rich than the coexisting olivine. Growth of the wadsleyite requires long-range Fe-Mg interdiffusion. If the transformation occurs out of equilibrium, by overstepping the equilibrium phase boundary in pressure, the same transformation can occur without a change in composition. In this case, growth of the wadsleyite is controlled by the rate of short-range diffusion across the interface between the two phases and is referred to as interface-controlled growth.

In a martensitic phase transformation, the mechanism does not involve nucleation and growth, but rather the rearrangement of atom positions by shearing. In this case, shearing results from the passage of partial dislocations and the product phase is related to the initial phase by a series of stacking faults. Martensitic transformations occur in metals where the new structure can be created by changing the layer stacking of the metal by shearing (*Porter and Easterling,* 1978). *Madon and Poirier* (1980) proposed that the olivine-ringwoodite transformation could occur by a martensitic-like mechanism, where the glide of partial dislocations on (100) of olivine would change the oxygen sublattice from hexagonal close-packed to cubic close-packed. This is not a true martensitic transition because a change in the oxygen sublattice from hexagonal to cubic close-packed is not enough to make the spinel structure. The shearing of the oxygen sublattice must be accompanied by shifting of the cations to new positions through a process known as "synchro-shear" (*Madon and Poirier,* 1980). *Burnley and Green* (1989) have shown that the transformation of Mg_2GeO_4-olivine to spinel can occur by this mechanism under conditions of relatively high shear stress.

2.10.1. Olivine transformations in meteorites. The ringwoodite that is readily observable by optical petrography in very highly shocked S6 chondrites occurs as polycrystalline aggregates that have the same chemical composition as the olivines in the same samples (*Chen et al.,* 1996; *Langenhorst et al.,* 1995). One may therefore infer that it formed via a solid-state transformation mechanism during shock compression (*Chen et al.,* 1996). Transmission electron microscopy examination of the polycrystalline ringwoodite in chondrites generally shows randomly oriented ringwoodite crystallites that range from about 100 nm (*Putnis and Price,* 1979; *Langenhorst et al.,* 1995) to several micrometers (*Chen et al.,* 1996) (Fig. 9). The random orientations and homogeneous distributions of ringwoodite crystallites suggest homogeneous intracrystalline nucleation throughout the olivine rather than heterogeneous nucleation on grain boundaries, which is the dominant mechanism at pressures closer to the equilibrium phase boundary (*Kerschhofer et al.,* 2000; *Mosenfelder et al.,* 2001). The presence of small amounts of glassy material in ringwoodites from Tenham (*Price et al.,* 1979) have been interpreted as remnants of a prograde high-density olivine glass that was an intermediate phase in the transformation of olivine to ringwoodite. However, such glassy phases have not been reported in more recent studies. In most samples, the ringwoodite composition is constant, implying that there was no Fe-Mg exchange during the transformation, and therefore the crystallites grew by interface-controlled growth rather than diffusion-controlled growth.

High-pressure experiments have been performed on hot-pressed olivine samples to determine reaction mechanisms and kinetics of the olivine-ringwoodite and olivine-wads-

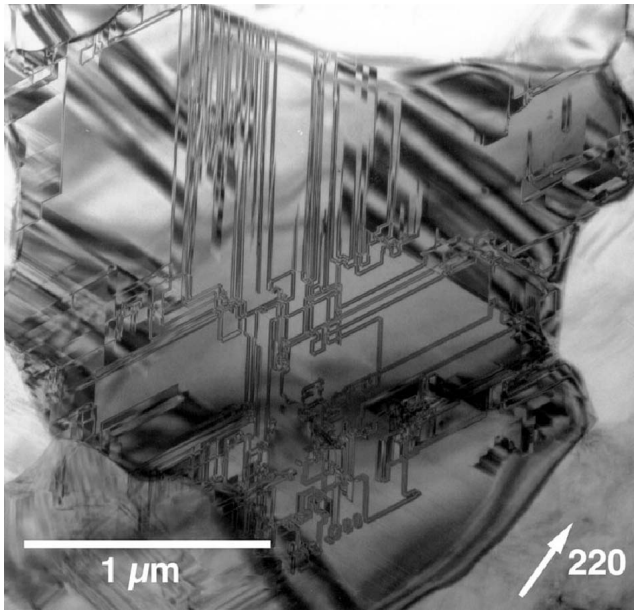

Fig. 9. Bright-field TEM image of a ringwoodite crystal in a large polycrystalline aggregate from Sixiangkou. The image was obtained using g = 220, which highlights the distinctive stacking faults on {110}.

leyite phase transformations (*Brearley et al.,* 1992; *Rubie and Ross,* 1994; *Sharp and Rubie,* 1995; *Kerschhofer et al.,* 1996, 1998, 2000). The dominant transformation mechanism was inferred to be incoherent grain boundary nucleation followed by interface-controlled growth. *Kerschhofer et al.* (1996) discovered a new intracrystalline mechanism that involved the formation of stacking faults in olivine on (100) followed by the nucleation of ringwoodite lamellae on the stacking faults. This produced the crystallographic relationship expected for the martensitic-like transformation mechanism, but clearly involved coherent heterogeneous nucleation followed by interface-controlled growth. *Chen et al.* (2004b) have discovered ringwoodite lamellae on $\{101\}_{ol}$ and $\{100\}_{ol}$ in partially transformed olivines in the Sixiangkou L6 chondrite, which they interpreted to have formed by the same mechanism as that described by *Kerschhofer et al.* (1996, 1998, 2000). However, these ringwoodite lamellae have a slightly higher fayalite content then the surrounding olivine, suggesting a diffusion-controlled growth mechanism rather than the interface-controlled growth mechanism described by *Kerschhofer et al.* (1996, 1998, 2000). The lamellae in Sixiangkou are also much coarser than those observed by *Kerschhoffer et al.* (1996, 1998, 2000). Detailed structural studies of the Sixiangkou ringwoodite lamellae are needed to determine the heterogeneous nucleation mechanism active in Sixiangkou and how it is related to those observed by *Kerschhofer et al.* (1996, 1998, 2000).

2.10.2. Enstatite transformations in meteorites. The transformation of pyroxene to its high-pressure polymorphs in shocked meteorites is less documented and more complicated than the olivine-ringwoodite transformations. In Sixiangkou, the majorite after enstatite (Fig. 10) consists of relatively large crystallites that are randomly oriented but contain subgrain boundaries (*Chen et al.,* 1996). The origin of the subgrain boundaries is not clear, but similar structures are observed in enstatite-pyrope composition garnets synthesized at high pressure and temperature and rapidly quenched (*Heinemann et al.,* 1997). The mechanism appears to be the same as that of ringwoodite: homogenous intracrystalline nucleation followed by interface-controlled growth. In the transformation of enstatite to akimotoite (*Tomioka and Fujino,* 1997), akimotoite occurs in a granular texture as well as in columnar texture where the crystals have a topotaxial relationship with the enstatite. The granular texture consists of randomly oriented crystallites from 100 to 200 nm, which is consistent with homogeneous intracrystalline nucleation and interface-controlled growth similar to that of polycrystalline ringwoodite. *Tomioka and Fujino* (1997) interpret the columnar texture as resulting from a martensitic-like mechanism. However, the TEM data presented by *Tomioka and Fujino* (1997) is also consistent with a coherent nucleation mechanism without martensitic-like shear. Enstatite in Tenham is also partially transformed to a granular intergrowth of 200-nm $MgSiO_3$-perovskite crystallites with the same chemical composition as the precursor enstatite (*Tomioka and Fujino,* 1997). This occurrence is also consistent with homogeneous nucleation and interface-controlled growth.

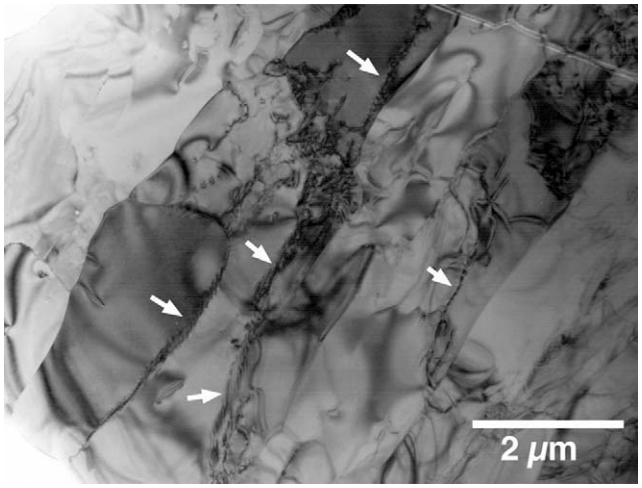

Fig. 10. Bright-field TEM image of a majorite crystal in a polycrystalline aggregate from Sixiangkou. The majorite crystals are >10 μm in size and contain numerous subgrain boundaries.

2.10.3. Plagioclase transformation in meteorites. The transformation of plagioclase to the hollandite structure, like the olivine and pyroxene transformations, occurs in and adjacent to shock melt. The hollandite consists of randomly oriented nanocrystals that range in size from 10 to about 100 nm (Fig. 11). Optically, the hollandite-structured plagioclase is isotropic and looks like maskelynite (diaplectic glass) or melted plagioclase (normal glass). The composition of hollandite-structured feldspars in meteorites ranges from $KaAlSi_3O_8$-rich (*Langenhorst and Poirier,* 2000a) to $NaAlSi_3O_8$-rich (*Gillet et al.,* 2000; *Tomioka et al.,* 2000) and intermediate-plagioclase compositions (*Langenhorst and Poirier,* 2000b; *Xie and Sharp,* 2004). The origins of these various hollandite aggregates have been interpreted

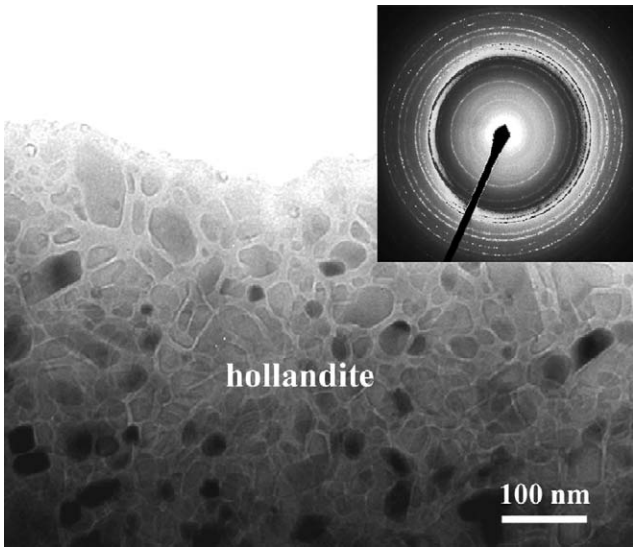

Fig. 11. Bright-field TEM image of nanocrystalline hollandite from Tenham. The individual crystallites range in size from 20 to 100 nm. The selected-area electron diffraction pattern contains diffraction rings that confirm the hollandite structure and indicate random orientations of the grains.

to be solid-state transformation (*Tomioka et al.,* 2000; *Langenhorst and Poirier,* 2000b; *Xie and Sharp,* 2004) and crystallization from melt (*Gillet et al.,* 2000). The nanocrystalline granular texture is consistent with both origins if the melt was a pure feldspar-composition liquid. If formed by a solid-state mechanism, the microstructure suggests homogeneous nucleation and interface-controlled growth, as in the formation of ringwoodite. If the polycrystalline hollandites in melt veins crystallized from feldspar-composition liquids during shock compression, the feldspar-composition liquid did not mix with the surrounding chondritic liquid, as one would expect if the liquids are miscible. This suggests that most of the transformation is via a solid-state mechanism. However, veins of hollandite extending away from polycrystalline aggregates in Sixiangkou indicate that at least some of the plagioclase was molten during shock. The distinction between solid-state transformation and liquid crystallization is an important consideration when using the presence of hollandite to constrain shock pressures.

2.10.4. Graphite transformation to diamond. The graphite-to-diamond transition is a special case. Here we summarize the detailed presentations of *DeCarli* (1995) and *DeCarli et al.* (2002a), which fully reference the relevant literature. As we noted earlier, both static and shock experiments indicate that the direct (uncatalyzed) transformation of disordered graphitic carbon to diamond requires pressures above ~15 GPa and transient high temperatures >3000 K. The resultant diamond is optically isotropic, mechanically strong, and polycrystalline, with randomly oriented crystallites from 20 nm (shock) to 50 nm (static). This reconstructive transformation is similar to the olivine-ringwoodite transition and involves homogeneous nucleation and growth. The diamond must be quenched at pressure to lower temperatures to avoid graphitization on pressure release. For lack of a better term, we will refer to it as HT (high-temperature) shock diamond. We do not preclude the possibility that HT shock diamond could be formed in a meteorite. To the best of our knowledge, however, all descriptions of meteoritic diamond appear to match the characteristics of diamond formed by a low-temperature mechanism in both static and shock experiments. The static flash heating experiments of *Bundy and Kasper* (1967) indicate that well-ordered graphite may be transformed at pressures above ~15 GPa and transient temperatures above ~1300 K. We will refer to the product as LT (low-temperature) shock or static diamond; 1300 K is a very low temperature relative to the melting point of graphite. The LT static diamond is a polycrystalline mixture of cubic and hexagonal (lonsdaleite) structures, optically anisotropic, and has a strong preferred orientation, with londaleite (100) parallel to (001) graphite. Although the preferred orientation and the low transformation temperature imply a martensitic mechanism, Bundy and Kasper noted that simple shear would not suffice to convert hexagonal graphite to either hexagonal or cubic diamond. The requirement for a minimum, albeit low, temperature requirement implies a thermally activated component in the transformation. The results of shock-recovery experiments on formation of LT shock diamond and studies of natural LT shock diamond from impact craters are in general accord with the static data. The common characteristics of the samples we have observed include optical anisotropy and strong preferred orientation. Distinct hexagonal (lonsdaleite) reflections are observed in some, but not all, terrestrial LT impact diamonds (*Koeberl et al.,* 1997). Laboratory shock experiments have also produced nanodiamond, cubic diamond particles having diameters in the range of 2–7 nm. These diamonds are structurally indistinguishable from the diamonds found in the detonation products of oxygen-deficient explosives and resemble the nanodiamonds found in carbonaceous chondrites.

Knowledge of the conditions for shock synthesis of LT diamond and for its subsequent survival can be used to estimate shock pressure in the surrounding rock or metal. The peak shock temperature of the graphite (which must be well-ordered) must be at least 1300 K, based on the static data. However, the temperature of the newly formed shock diamond and the surrounding rock and metal must be less than 2000 K on release of pressure, if graphitization of the diamond is to be avoided. Graphite has a very low shock impedance; shock pressure equilibration with the matrix will be achieved via a sequence of shock reflections. As we pointed out earlier, in the discussion of shock reflections and loading path effects, shock temperature in the graphite will depend on the loading path. Based on the simple geometry illustrated in Fig. 5, we have calculated shock temperature in graphite as a function of continuum pressure in various matrices. For graphite in iron-nickel meteorites, continuum pressures in the iron in the range of 60–120 GPa correspond to shock temperatures in the graphite in the range of 1300–2000 K. The calculated temperature of the iron on release from 120 GPa will be <1700 K. For graphite in granite or quartzite, the continuum pressure range of ~27–38 GPa corresponds to the 1300–2000 K graphite shock-temperature range. This suggests that graphite is more likely to transform to diamond where it is surrounded by minerals with low shock impedance. There are several caveats. The shock-temperature calculations are based on a simple geometric model of the graphite inclusion and shock propagation normal to the plane of the inclusion. In a more realistic geometry the shock temperature in the graphite could be nonuniform. One must also consider the possibility of chemical reactions or diffusion between hot diamond and hot matrix, e.g., diffusion of carbon in iron or reaction of diamond with a molten silicate. These considerations may further narrow the pressure range over which shock synthesis of LT diamond is possible. *El Goresy et al.* (2001) observed in Ries Crater gneiss that impact diamond seemed to be preferentially found in contact with garnet grains, and they infer that the reflected shock from the higher-shock-impedance garnet was responsible for the transformation. However, other interpretations are possible. The garnet may have served as a heat sink that preserved the adjacent diamond from graphitization. Low-temperature shock diamond has been found in heavily shocked iron meteorites and is commonly found in ureilites. The characteristics of LT shock diamond are distinctive and are unlike the charac-

teristics of either terrestrial mantle diamond or low-pressure CVD diamond. The presence of LT shock diamond in some samples of the Canyon Diablo meteorite is correlated with metallographic evidence of high shock pressures in the range above 60 GPa (*Lipschutz,* 1968).

2.11. Transformation Kinetics and Temperature

Nucleation and growth has only been discussed as a viable mechanism for the shock transformation of olivine to ringwoodite by relatively few authors (e.g., *Chen et al.,* 1996, 2004b; *Ohtani et al.,* 2004; *Xie and Sharp,* 2004) because it has been assumed by many that the shock events that produced reconstructive phase transitions in meteorites were too short in duration for such a complex kinetic process. An alternative explanation, based on the presence of interstitial glass, is that the shock event initially produces a high-density prograde glass that subsequently devitrifies to form high-pressure minerals (*Price et al.,* 1979). One problem with this interpretation is that it is difficult to prove that interstitial glass is prograde rather than retrograde. Like the direct transformation, it still requires nucleation and growth of the high-pressure phases during shock compression because solid-state devitrification at low pressure would require temperatures too high for metastable high-pressure minerals to form. The textural evidence for homogeneous nucleation and interface-controlled growth in many polycrystalline high-pressure silicates in melt veins indicate that the shock pulses that caused the transformations in natural samples were of relatively long duration, perhaps up to several seconds (*Ohtani et al.,* 2004; *Chen et al.,* 2004b). The microsecond durations typical of shock experiments, combined with the relatively low shock temperatures produced in shock-recovery experiments, explain why such experiments have not produced high-pressure polymorphs of olivine and pyroxene. The kinetics of such reconstructive phase transformations are simply too slow under conditions of shock-recovery experiments.

Because reconstructive phase transitions in silicates are kinetically sluggish and require high temperatures to overcome the large activation barriers, the transformations that occur in meteorites are strongly dependent on temperature as well as pressure. The shock calibration of *Stöffler et al.* (1991) stresses shock pressure as the primary driver of shock-metamorphic effects and does not discuss temperature effects or reaction kinetics. Static high-pressure kinetic experiments have shown that dry hot-pressed San Carlos olivine transforms to ringwoodite, on an observable timescale, only above 900°C at 18–20 GPa (*Kerschhofer et al.,* 1996, 1998, 2000). The transformation of enstatite to akimotoite is even more sluggish, requiring temperatures in excess of 1550°C for transformation at 22 GPa (*Hogrefe et al.,* 1994). The fact that some olivine and low-Ca pyroxene in meteorites transform to high-pressure polymorphs by nucleation and growth indicates that shock temperatures of the transformed material must have been much higher than the temperatures in the static experiments. This is supported by the observation that solid-state transformations of olivine and pyroxene occur almost exclusively within or in close proximity to shock melt, which represents the hottest part of the sample during shock. Although some solid-state phase transitions may occur in response to localized and transient pressure spikes during the passage of the shock front (*Kieffer,* 1971), the transformations associated with mesoscale shock melting is not limited to the microsecond timescales of transient shock pressures. The ubiquity of transformed silicates within and along shock veins in S6 samples and the spatial scale of transformation indicate that high temperatures associated with melting provide the energy to overcome the kinetic barriers to nucleation and growth of the high-pressure phases. Because the elevated temperatures of the melt-vein regions can last up to about 1 s, the solid-state transformations that occur in and along melt veins are likely to have formed at the equilibrated shock pressure rather than during transient pressure spikes.

2.12. Pressure Constraints from Solid-State Transformations

The use of high-pressure solid-state phase transitions to quantitatively calibrate shock pressures in natural samples is problematic because most of the shock-induced transitions are reconstructive and kinetically sluggish. The fact that olivine and pyroxene do not transform to their high-pressure polymorphs in shock-recovery experiments has been used by *Stöffler et al.* (1991) as evidence that extreme pressure is needed to transform them in meteorites. The key questions are: How important is pressure in driving phase transitions, and what effect does pressure have on reaction kinetics?

The driving energy for nucleation is provided by the volume free energy change ΔG_v of forming the nuclei. Nucleation rates are controlled by the activation energy of nucleation, which is proportional to the inverse square of the free energy change. For the transformation of a low-pressure phase to a high-pressure polymorph, overstepping the phase boundary in pressure rapidly decreases the activation energy for nucleation. All such transformations require some pressure overstepping for nucleation to occur, but there is little nucleation rate data available for phase transitions in silicates. Experimental kinetic data for the olivine-wadsleyite and olivine-ringwoodite transformations are only available for incoherent nucleation on grain boundaries (*Rubie and Ross,* 1994; *Brearley et al.,* 1992; *Kubo et al.,* 1998a,b; *Liu et al.,* 1998) and for coherent intracrystalline heterogeneous nucleation (*Kerschhofer et al.,* 1996, 1998, 2000). There is no experimental data for intracrystalline homogeneous nucleation, which appears to be the mechanism most common in meteorites. For incoherent grain-boundary nucleation, little pressure overstepping is required and nucleation rates are assumed to be very fast (*Mosenfelder et al.,* 2001). Because the activation barrier for intracrystalline homogeneous nucleation should be higher, larger pressure overstepping is expected.

In studies of olivine-ringwoodite transformation kinetics, growth rather than nucleation is the dominant rate-con-

trolling step (*Rubie,* 1993; *Mosenfelder et al.,* 2001). The rate equation for interface-controlled growth is given by

$$\dot{x} = k_0 T \exp[-(\Delta H_a + PV^*)/RT][1-\exp(\Delta G_r/RT)]$$

where $\dot{x}$ is the growth rate, k_0 is a constant, ΔH_a is the activation enthalpy, V* is the activation volume for growth, ΔG_r is the free energy change of reaction, and R is the gas constant. The first part of the equation is an Arrhenius term that describes the thermally activated diffusion of atoms across the interface. The second part is a thermodynamic term that describes the driving force for growth. Many experimental studies have provided kinetic data for interface-controlled growth in the olivine-spinel transformation (for reviews, see *Rubie,* 1993; *Mosenfelder et al.,* 2001). The temperature dependence of growth is given by the activation enthalpy, which is approximately 350 to 400 kJ mol^{-1} (*Mosenfelder et al.,* 2001). This indicates a strong temperature dependence, which is consistent with the requirement of T > 900°C for observable transformation of dry olivine in quench experiments. The pressure dependence of growth is given by the activation volume V*. *Kubo et al.* (1998a) have used *in situ* transformation experiments to constrain the value of V* to between 0 and 4 cm^3 mol^{-1}, whereas *Rubie and Ross* (1994) estimate V* to range from 12 cm^3 mol^{-1} at 1 bar and 4 cm^3 mol^{-1} at 15 GPa. These positive activation volume estimates indicate that interface-controlled growth rates decrease with increasing pressure. This also suggests that the olivine-ringwoodite transformation that occurs in naturally shocked meteorites should require increasingly higher temperatures with increasing pressure. The fact that olivine and pyroxenes do not transform at very high pressures in diamond anvil experiments without being heated to very high temperatures further supports the idea that high temperatures actually control the distribution of olivine and pyroxene high-pressure polymorphs in chondrites.

Phase equilibrium data from static high-pressure experiments can be used to provide only limited constraints on pressure. The actual phase transitions are commonly metastable, involving polymorphs that are not in stable equilibrium. For example, the post-stishovite phase of SiO_2 known as seifertite (the α-PbO_2 structure) in Shergotty formed directly from either cristobalite or tridymite although there is no stable equilibrium between these phases. The equilibrium phase boundary between the $CaCl_2$ structure and the α-PbO_2 structure, at around 80 GPa, is irrelevant and one must consider the metastable boundaries between either cristobalite and seifertite or tridymite and seifertite. Because these metastable boundaries occur at a lower pressure than the $CaCl_2$-seifertite equilibrium boundary, the minimum transformation pressure is actually much lower than the 80 GPa pressure that one would infer from the minimum stability (*El Goresy et al.,* 2000).

The olivine-ringwoodite, enstatite-majorite, enstatite-akimotoite, and enstatite-$MgSiO_3$-perovskite phase transitions are all metastable. In all these cases, the metastable phase boundaries of interest are lower in pressure than the minimum pressure of stable equilibrium. The phase relations only limit the pressure to be greater than the metastable equilibrium between the low- and high-pressure polymorphs. This issue is especially important for ringwoodite, which is commonly used to indicate S6 shock conditions and pressures in excess of 50 GPa in shocked chondrites (*Stöffler et al.,* 1991). The pressure overstepping required to form ringwoodite is dependent on both the temperature and the time available for the transformation. The fact that ringwoodite has never been synthesized in a shock-recovery experiment is a result of the very short durations of those experiments, combined with the relatively low temperatures that result from using high-impedance containers. However, ringwoodite that occurs in or adjacent to shock melt in S6 chondrites formed at temperatures much higher than those in shock-recovery experiments and over a shock duration that may exceed the experimental shock duration by 5 orders of magnitude. Ringwoodite in shocked chondrites must form at pressures in excess of the metastable phase boundary (~18 GPa), but the amount of pressure overstepping required in nature is not constrained by shock or static high-pressure experiments. An alternative means of constraining shock pressures in meteorites is needed.

2.13. Constraints on Shock Pressure from Melt-Vein Crystallization

Shock-induced melt veins are common in moderately shocked chondrites of shock stage S3–S4 and ubiquitous in highly shocked S5–S6 chondrites. They occur as thin black veins, from 1 μm to several millimeters wide (*Stöffler et al.,* 1991). *Fredriksson et al.* (1963) used shock experiments to demonstrate that these melt veins are indeed the result of shock melting. Shock veins can form by shock-wave collisions, as discussed above, by frictional heating along shear bands, analogous to pseudotachilites, or by the collapse of open fractures or pores during shock compression. Shock veins are of critical importance in the interpretation of shock transformation effects because they are the locations of nearly all crystalline high-pressure minerals that occur in shocked meteorites and the exclusive locations of S6 shock effects.

An alternative to using deformation and solid-state transformation effects to constrain shock pressures is to use the crystallization of high-pressure minerals from the shock-induced melt combined with experimental high-pressure melting relations. This approach was first used by *Chen et al.* (1996), who used TEM to determine melt-vein assemblages in Sixiangkou. They found that the chondritic melt in a large melt vein crystallized to form majoritic garnet and magnesiowüstite (Fig. 12), which, based on the phase diagram of the CV3 chondrite Allende (*Agee et al.,* 1995), is stable at pressures between about 22 and 27 GPa (Fig. 13). *Chen et al.* (1996) inferred a crystallization pressure of about 25 GPa, which is half the value of the low-pressure threshold for S6 shock conditions of *Stöffler et al.* (1991).

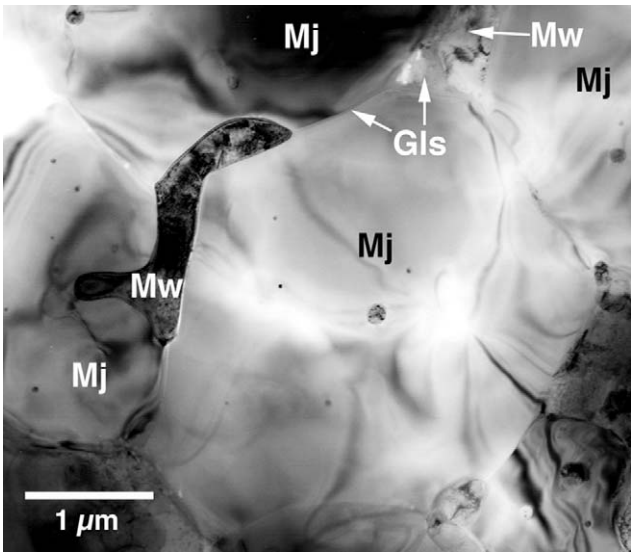

Fig. 12. Bright-field TEM image of majoritic garnets and magnesiowüstite that crystallized in a melt vein in the Sixiangkou L6 S6 chondrite.

Using melt-vein crystallization to estimate shock pressure is controversial in the field of shock metamorphism because it uses phase equilibrium data obtained in static high-pressure experiments. However, there are several reasons why high-pressure melting relations can be applied to the interpretation of melt-vein crystallization. First, the most common melt-vein assemblage seen in S6 chondrites, majorite plus magnesiowüstite, is also produced in static high-pressure melting experiments on both Allende (*Agee et al.,* 1995) and on Kilburn-hole-1 peridotite (*Zhang and Herzberg,* 1994). The textures and crystal sizes in the centers of large chondritic melt veins, such as those in Tenham, Sixiangkou, and RC 106 (*Chen et al.,* 1996; *Aramovich et al.,* 2003; *Xie et al.,* 2005), are very similar to the textures and crystal sizes produced in the static experiments (*Agee et al.,* 1995). Similarly, the chemical compositions of the crystallized majoritic garnets are very similar to the compositions of garnets in the experiments (*Chen et al.,* 1996). Compared to solid-state reconstructive phase transitions, melt-vein crystallization involves much smaller kinetic barriers.

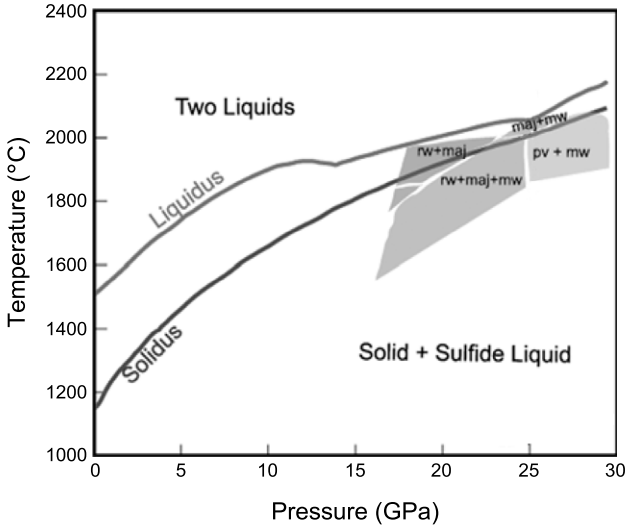

Fig. 13. The crystallization-pressure regions illustrated on a simplified version of the Allende phase diagram (*Agee et al.,* 1995); rw = ringwoodite, maj = majorite, mw = magnesiowüstite, pv = perovskite.

Melt-vein crystallization has a great advantage over solid-state transformation for constraining shock pressure histories. Because the cooling produced by adiabatic pressure release is relatively small, shock melt cools predominantly by conduction to the surrounding, relatively cool, host meteorite. This results in crystallization that starts at the vein margins and moves inward to the melt-vein core as crystallization proceeds. The resulting crystallization sequence provides a record of shock pressure through time. As we will discuss below, this record can be several hundred milliseconds long. If the recorded pressure-temperature-time history exceeds the period of elevated pressure, crystallization assemblages should record the pressure release.

An important aspect of using melt-vein mineralogy to constrain pressure is that melt veins do not crystallize at equilibrium. Silicate liquids must be supercooled relative to the liquidus in order to provide the free energy to overcome the activation energy of nucleation and growth. Unlike the case of solid-state transformations, melt-vein crystallization occurs at very high temperatures, on the order of 2000° to 2400°C at 25 GPa for Allende and KLB-1, respectively (*Agee et al.,* 1995; *Zhang and Herzberg,* 1994). At these temperatures, diffusion and crystal growth rates can be very rapid and therefore the kinetic barriers for crystallizing high-pressure minerals are much lower than those for solid-state transformations. Contrary to the pressure overstepping needed for solid-state transformations, the supercooling of silicate liquid does not require excess pressure to form high-pressure phases, so pressure constraints from melt-vein crystallization are likely to provide lower and more accurate pressure estimates that phase transformations calibrated against shock-recovery experimental results.

A limitation of the melt-vein approach is that the mineral assemblage that crystallizes may not be the equilibrium assemblage inferred from the static high-pressure experiments. Crystallization of metastable phases such as akimotoite, which is a subsolidus phase in the Mg_2SiO_4-$MgSiO_3$ system (*Gasparik,* 1992), occurs along the margins of melt veins in Tenham (Fig. 14) where the melt-vein quench rate was highest and therefore the supercooling was large (*Xie et al.,* 2005). However, the central core of the same melt veins contains the majorite plus magnesiowüstite assemblage that is inferred to be the equilibrium assemblage in the high-pressure experiments. It appears that the melt-vein margins and very thin melt veins, which are most rapidly quenched, are most likely to contain metastable crystallization products. In using melt-vein mineralogy to constrain crystallization and shock pressure, it is not appropriate or

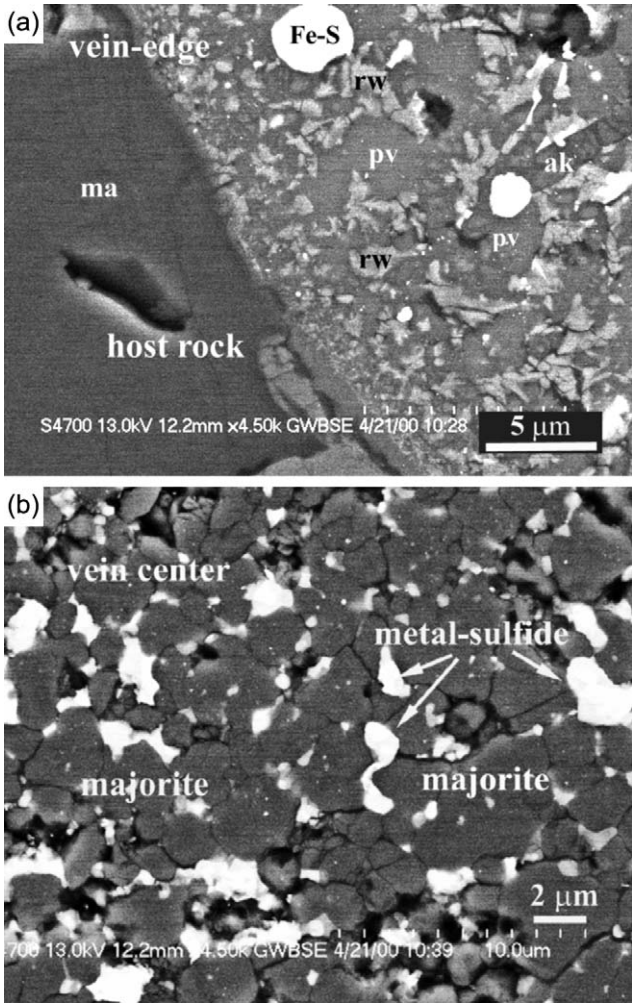

Fig. 14. Field-emission SEM images of a melt vein in Tenham. The melt-vein margin (top) contains ringwoodite (rw), akimotoite (ak), and vitrified silicate perovskite (pv) along with solidified droplets of Fe-sulfide melt. The vein core (bottom) contains the common assemblage of majorititic garnet and magnesiowüstite along with blebs of solidified metal-sulfide melt.

necessary to assume that crystallization was an equilibrium process. Like solid-state transformations, melt-vein assemblages provide constraints on crystallization pressure rather than precise pressure determinations. Because kinetic barriers for crystallization are less than for reconstructive phase transformations, it is likely that crystallization pressure can be more accurately calibrated.

2.14. Crystallization Pressure vs. Shock Pressure

A key issue in the use of melt-vein assemblages for constraining shock pressure is the relationship between crystallization pressure and shock pressure. This relationship is determined by when the melt vein crystallizes relative to shock loading and pressure release. Thermal modeling of melt-vein quench shows that a 1-mm-wide melt vein requires hundreds of milliseconds to crystallize (*Langenhorst and Poirier,* 2000a; *Xie et al.,* 2003, 2005), whereas transient pressure heterogeneities equilibrate in about 1 μs for a sample with a 1-mm grain size. Therefore, nearly all the melt-vein crystallization occurs after pressure equilibration such that the pressure history recorded by melt-vein crystallization does not include transient pressure spikes. Small-scale transformation effects, such as those described by *Kieffer* (1971), record the transient pressure history and are therefore not as useful for determining the equilibrated shock pressure. The timing of melt-vein crystallization relative to pressure release is equally important. One might argue that the relatively low pressure of melt-vein crystallization in S6 chondrites compared to the S6 calibration pressure of *Stöffler et al.* (1991) indicates that crystallization occurs upon pressure release from an equilibrated shock pressure in excess of 50 GPa. Such a hypothesis can be easily tested by looking at the sequence of minerals that crystallize from the melt-vein edge to the melt-vein core. Because the crystallization history of the melt vein is recorded from rim to core, the assemblages across large melt veins should record such a pressure release. This is the case for Zagami (*Langenhorst and Poirier,* 2000b), but clear evidence for crystallization during pressure release is lacking for highly shocked chondrites such as Tenham (*Xie et al.,* 2005) and RC 106 (*Aramovich et al.,* 2003). If crystallization occurred during pressure release for these S6 chondrites, then the pressure release was only ~5 GPa over the relatively long duration (50–250 ms) of cystallization.

The crystallization assemblages in a given melt vein will depend on the time required for melt vein quench vs. the duration of high shock pressures (Fig. 15). If the shock duration were longer than the crystallization time of the melt vein, then we would expect crystallization to have occurred during the period of high shock pressure and therefore record the continuum shock pressure. This appears to be the case for S6 samples such as Tenham (*Langenhorst et al.,* 1995; *Xie et al.,* 2003, 2005), RC 106 (*Aramovich et al.,* 2003), and Sixiangkou (*Chen et al.,* 1996). If the shock duration was the same duration as melt-vein crystallization, then it is likely that melt-vein crystallization would record both the continuum shock pressure and a lower pressure of partial release such that the core of the vein might contain an assemblage that crystallized at a lower pressure than that of the rest of the vein. If the shock pulse were shorter than the melt-vein quench time, one would expect crystallization of low-pressure assemblages in the core of the melt vein. This appears to be the case for S4 samples Kunashak and La Lande, which contain plagioclase-bearing crystallization assemblages. Finally, we note that some veins may form at low pressure during pressure release. The mineralogy of these veins would be unrelated to either the magnitude or duration of peak shock pressure.

2.15. Thermal Modeling of Melt-Vein Quench

The thermal history recorded in melt veins can be extracted by modeling the thermal history of the vein as it quenches and crystallizes (*Langenhorst and Poirier,* 2000a; *Xie et al.,* 2005). Finite-element methods can be used to

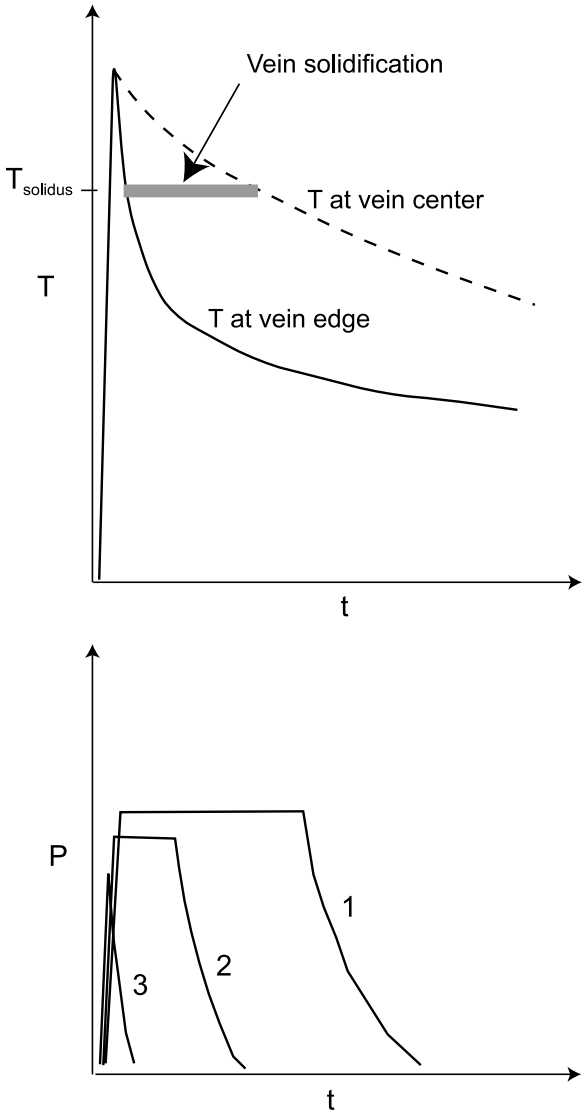

Fig. 15. The temperature profile (top) illustrates the cooling history of the melt-vein edge (solid) and melt-vein center (dashed) as they pass through the solidus temperature. The pressure-time profile (bottom) illustrates three quench scenarios: (1) The pressure pulse exceeds the duration of the total quench time and crystallization occurs at equilibrium shock pressure. (2) The pressure pulse is shorter than the total quench time, resulting in quench through the equilibrium shock pressure and into pressure release. (3) The pressure pulse is much shorter than the total quench time such that most of the quench occurs after pressure release.

model heat transfer to calculate transient heat flow from the melt vein into the chondrite matrix. The temperature difference between the melt vein and the surrounding is estimated by assuming that the melt-vein temperature is above the liquidus at pressure, and calculating the bulk shock temperature of host rock by using the method described above and in Appendix A. The thermal modeling allows one to calculate the temperature of any point within or near the melt vein as a function of time. The total crystallization time for the vein is estimated by calculating the time difference between when the melt-vein center and margin pass through the solidus temperature. This approach has been used to estimate a 50-ms time required to crystallize a 580-μm melt vein in Tenham (*Xie et al.,* 2003, 2005) (Fig. 16).

2.16. Application to Melt Veins in S3–S6 Chondrites

Melt-vein assemblages have been determined for a variety of S6 chondrites including Sixiangkou (*Chen et al.,* 1996), Acfer 040 (*Sharp et al.,* 1997), Tenham (*Xie et al.,* 2005), and RC 106 (*Aramovich et al.,* 2003). Similarly, a series of S3–S5 samples, including Umbarger (*Xie and Sharp,* 2004), Roy, La Landa, and Kunishack have been characterized. The melt-vein assemblages correspond to crystallization over a wide range of pressures from less than 3 GPa (La Landa and Kunishack) to approximately 25 GPa for the S6 samples. These results suggest that the maximum crystallization pressures, and therefore shock pressures, of L chondrites are around 25 GPa. Samples such as Acfer 040 (*Sharp et al.,* 1997) and Tenham (*Xie et al.,* 2005) have melt-vein assemblages that include silicate-perovskite, which is stable above 23 GPa (*Chen et al.,* 2004a). However, the perovskite in both these samples occurs with ringwoodite, suggesting that the pressure was not much greater than 23 GPa. This lack of evidence for melt-vein crystallization above 25 GPa indicates that the calibration of S6 shock effects of *Stöffler et al.* (1991) is about two times too high. A maximum shock pressure of about 25 GPa for chondrites also suggests that either the impact velocities in the early solar system are relatively low, or that samples shocked to significantly higher pressures have not been recognized. Using the synthetic Hugoniot for Tenham and assuming an impact between two Tenham-like bodies, one can calculate that a

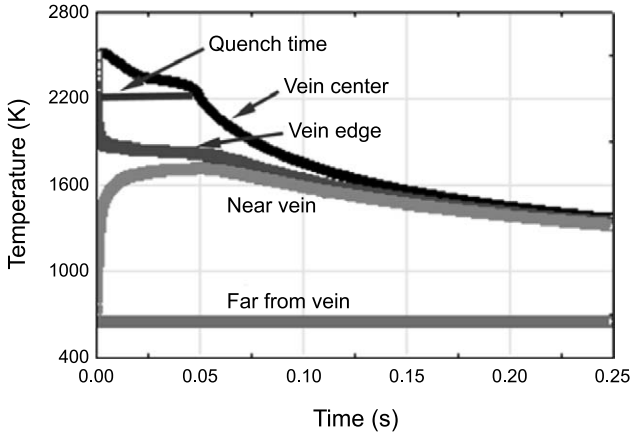

Fig. 16. Temperature vs. time profiles for the vein center, vein edge, and host rock for the 580-μm-wide vein in Tenham. The quench duration is the lag time between crystallization of vein edge and vein center, which is ~50 ms. The distances from vein-host interface to vein center, vein edge inside the vein margin, host rock near but outside the vein, and host rock outside the vein are 0.29 mm, 0.02 mm, 0.04 mm, and 4 mm respectively.

pressure of 25 GPa corresponds to a relative impact velocity of ~2 km/s (*Xie et al.,* 2005). Alternatively, the 25-GPa samples may have sampled a part of the parent body that was relatively far from the impact site and therefore experienced a lower continuum shock pressure than that near the impact site. If this were the case, one would expect to see chondrites that are more highly shocked than the S5–S6 samples that have been studied to date. It is possible that the more highly shocked samples exist, but high postshock temperatures have annealed out shock metamorphic features and transformed high-pressure minerals back to their low-pressure polymorphs. *Rubin* (2004) has provided evidence for nearly complete annealing of shock features in ordinary chondrites that had been previously shocked. Much more work is needed to determine shock pressures and durations that affected meteorites. Only after shock pressures are well known can we constrain the velocities of impact on meteorite parent bodies.

APPENDIX A: SPREADSHEET CALCULATIONS

In this section, we present a specific example of spreadsheet shock wave calculations. All the operations are based on equations (1)–(7) in the theory section. We use the formula notation of Excel in this section.

In column A, labeled U_p, increment particle velocity from 0 in steps of 0.01 km/s (0.00, 0.01, 0.02 . . .) up to 5 km/s. The increment of 0.01 is arbitrary, chosen because it provided adequate resolution; the upper particle velocity limit of 5 km/s covers the pressure range in excess of 100 GPa for meteoritic minerals.

In column B, U_s (shock velocity), enter the formula: = C + s * Ax, where C and s are the equation of state parameters of equation (7), and Ax is the column reference. *Ahrens and Johnson* (1995a) list the following equation of state parameters for Stillwater bronzitite: $U_s = 5.99 + 1.56 * U_p$ (for $U_p <$ 0.483 km/s), $U_s = 6.47 + 0.6 * U_p$ (for 0.483 km/s < $U_p <$ 2.131 km/s), and $U_s = 5.16 + 1.17 * U_p$, (for 2.043 km/s < $U_p <$ 3.481). Note that the particle velocity ranges in parentheses refer to the data range over which the straight line fit was made and not to a range of validity. Hugoniot measurements on other pyroxenes indicate no anomalies in the particle velocity range between 3.5 km/s and 5 km/s. It is therefore probably safe to extrapolate the Stillwater bronzitite Hugoniot to a particle velocity of 5 km/s.

For efficiency, one can enter the first equation in column B, the second in column C, and the third in column D. The fill operation is used to calculate all three relationships over the entire range of particle velocities. By inspection, one can determine the smoothest crossover points. The column C equation is entered in column B at the first crossover particle velocity (0.50 km/s, in this case), and the column D equation is entered in column B at the second crossover velocity (2.30 km/s). Columns C and D may now be overwritten.

In column C, P (pressure), enter the formula = ρ_0 * Ax * Bx, (equation (2); neglecting P_o, atmospheric pressure in this case) where ρ_0 is the initial density and Ax and Bx are column references to U_p and U_s. Note: If U_s and U_p have units of km/s and ρ has units of Mg/m^3, P has the dimensions of GPa. Also note that g/cm^3 and Mg/m^3 are numerically equal.

In column D, V (specific volume at pressure P), enter the formula = $1/\rho_0$–Ax^2/Cx (from equation (4), neglecting P_o). At this point, one may plot the Hugoniot data in P–V, P–U_p, P–U_s, or U_s–U_p planes.

One may also calculate the internal energy increase on shock compression, E–E_o in column E by entering the formula = 0.5 * Cx * ($1/\rho_0$–Dx) (equation (6), neglecting P_o). Note that E–E_o has dimensions of kJ/g or the numerically equal MJ/kg.

The area under the Hugoniot, an approximation to the area under the release adiabat, may be calculated by a Simpson's rule integration in column F. The first entry in the column is 0. The second entry is the formula = 0.5 * (Cx + Cx_{-1})*(Dx_{-1}–Dx) + Fx_{-1}, e.g., F10 = 0.5 * (C10 + C9) * (D9–D10) + F9.

The waste heat, column G, is given by the formula = Ex–Fx.

A portion of the spreadsheet is shown in Table A-1.

In column G, one may note that the waste heat on release from a pressure of 50.27 GPa is 223 J/g. It is useful to know that for most common minerals, excluding metals, the average specific heat over the temperature range between 300 K and 1000 K is ~1 J/gK. Assuming a preshock temperature of 300 K, one might estimate the postshock temperature to be ~525 K, ±~60 K. For a more precise estimate of postshock temperature, one would consult a table of H_t–H_{298} for the specific mineral over the temperature range of interest.

The corresponding shock temperature may be estimated from the approximate relationship:

Tshock = T_o * e^ (Γ*(V_o–V)), where To is the waste heat temperature (in K) and Γ is the Grüneisen parameter, a function of thermal expansion, bulk modulus, specific volume and C_v, the heat capacity at constant volume. High-pressure data on Γ are sparse, but for most rocks and minerals over the pressure range up to about 100 GPa, estimated values of Γ are in the range of 0.5 to about 2. Using a Γ of 1 and a postshock temperature of 525 K, the calculated shock temperature would be ~565 K. With a Γ of 2, the calculated shock temperature would be ~615 K. These calculations support the general argument that the reduction of temperature is relatively small on adiabatic expansion from high shock pressures.

Constructing Synthetic Hugoniots

The Hugoniot data compilations of *Ahrens and Johnson* (1995a,b) are relatively complete. Only a few mineral or rock Hugoniots have been published subsequently. One may

TABLE A-1.

A	B	C	D	E	F	G
Stillwater ρ = 3.277 (U_p, km/s)	Bronzitite (U_s, km/s)	P, GPa	Specific Volume (cc/g)	Internal Energy Increase ($E–E_o$, kJ/g)	Recoverable Energy Area under Hugoniot (kJ/g)	Waste Heat (kJ/g)
2	7.67	50.26918	0.225585	2	1.776532311	0.223467689
2.01	7.676	50.56005	0.22525	2.02005	1.793438821	0.226611179
2.02	7.682	50.85131	0.224915	2.0402	1.810416376	0.229783624
2.03	7.688	51.14296	0.224581	2.06045	1.827464866	0.232985134
2.04	7.694	51.43501	0.224247	2.0808	1.84458418	0.23621582
2.05	7.7	51.72745	0.223914	2.10125	1.861774208	0.239475792

note that Hugoniot data are not available for many mineral compositions of interest to meteorite researchers. Hugoniot data are available for only a few olivine, pyroxene, and feldspar compositions. However, available data indicate that Hugoniots are not too sensitive to compositional differences in isomorphous mineral series. The P–U_p Hugoniots of forsterite and fayalite are closely matched, the P–U_p Hugoniots of various feldspars are closely matched and P–U_p Hugoniots of various pyroxenes are also closely matched. In the absence of Hugoniot data on the specific mineral composition of interest, one is forced to pick the closest match available.

However, there are a few minerals for which no Hugoniot data exist. We have noted that most rocks and minerals have small coefficients of thermal expansion to justify our use of the Hugoniot to approximate the release adiabat. By the same argument, one may use isothermal P–V data from static compression experiments to approximate Hugoniots, using equations (4) and (5) to convert P–V data to U_s–U_p and P–U_p planes. If the material of interest is a polymineralic rock, one may construct a P–V relationship for the rock by summing the volumes of the constituent minerals at pressure. (*Ahrens and Johnson,* 1995b). Shock wave workers have been using this technique for over 50 years because it works well in the pressure range above about 10 GPa, where material strength effects may be neglected. The agreement has been excellent between measured Hugoniots and synthetic Hugoniots. In the most extreme example, the measured Hugoniot of brucite is a good match in the pressure regime above 10 GPa to the Hugoniot synthesized by volume addition of MgO and water Hugoniots. One may also synthesize the Hugoniot of a porous material, allowing the initial porosity to crush up over an appropriate range of pressures. Since the Hugoniot range of interest would probably be above 10 GPa, one could simply let the porosity crush up linearly over the range of 0–5 GPa. The details of the crushup would have no effect on the Hugoniot above the crushup range. Note that initial porosity has a much greater effect on a Hugoniot than compositional differences. *Anderson and Ahrens* (1998) reported measurements of the Hugoniot of Murchison. They noted that their measurements disagreed with the Hugoniot calculated by simple addition at pressure of the volumes of the constituent minerals. However, rather than measuring porosity, they used mineral norms and composition data to calculate a porosity of 16%. Measured values of Murchison porosity cluster around 23%. If one uses 23% porosity in calculating the Hugoniot of Murchison, there is excellent agreement between measured and calculated Hugoniots.

Figure A-1 depicts P–U_p Hugoniots of some chondritic minerals and a synthetic Hugoniot for Tenham.

Meteoritic iron, represented by the Hugoniot for Fe-10%Ni, has the highest shock impedance over the entire pressure range considered here. However, relative shock impedances can change with pressure. At 10 GPa, the shock impedances of troilite and albite are closely matched. At about 55 GPa, the shock impedance of troilite becomes higher than the shock impedance of fayalite. The synthetic Hugoniot of Tenham, calculated by volume addition of its components, is very close to the Hugoniot of forsterite. The closeness of the Hugoniots of fayalite and forsterite illustrates the relative insensitivity of P–U_p Hugoniots to the

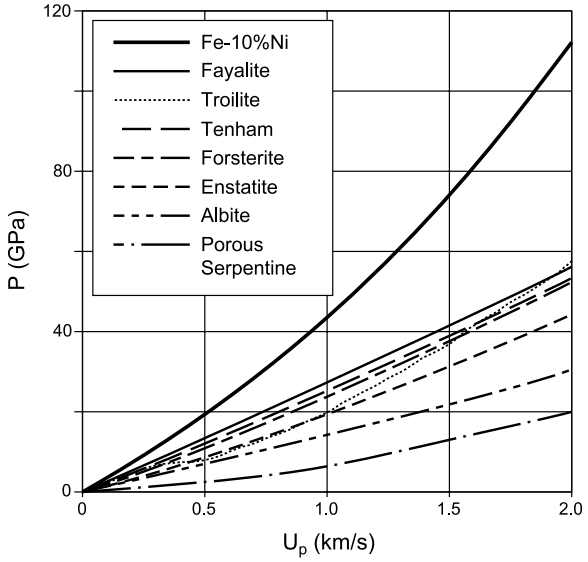

Fig. A-1. P–U_p Hugoniots of some chondritic minerals and a synthetic Hugoniot for Tenham.

substitution of Fe for Mg in isomorphous series. Finally, the Hugoniot for porous serpentine is a proxy for a typical carbonaceous chondrite Hugoniot.

REFERENCES

Agee C. B., Li J., Shannon M. C., and Circone S. (1995) Pressure-temperature phase diagram for the Allende meteorite. *J. Geophys. Res., 100,* 17725–17740.

Ahrens T. J. and Gaffney E. S. (1971) Dynamic compression of enstatite. *J. Geophys. Res., 76,* 5504–5513.

Ahrens T. J. and Gregson V. G. (1964) Shock compression of crustal rocks: Data for quartz, calcite, and plagioclase rocks. *J. Geophys. Res., 69,* 4839–4874.

Ahrens T. J. and Johnson M. L. (1995a) Shock wave data for minerals. In *Mineral Physics and Crystallography: A Handbook of Physical Constants* (T. J. Ahrens, ed.), pp. 143–184. American Geophysical Union, Washington, DC.

Ahrens T. J. and Johnson M. L. (1995b) Shock wave data for rocks. In *Rock Physics and Phase Relations: A Handbook of Physical Constants* (T. J. Ahrens, ed.), pp. 35–44. American Geophysical Union, Washington, DC.

Ahrens T. J. and Rosenberg J. T (1968) Shock metamorphism: Experiments on quartz and plagioclase. In *Shock Metamorphism of Natural Materials* (B. M. French and N. M. Short, eds.), pp. 59–81. Mono, Baltimore.

Ahrens T. J., Lower J. H., and Lagus P. L. (1971) Equation of state of forsterite. *J. Geophys. Res., 76,* 518–528.

Alder B. J. (1963) Physics experiments with strong pressure pulses. In *Solids Under Pressure* (W. Paul and D. W. Warshauer, eds.), pp. 385–420. McGraw-Hill, New York.

Anderson W. W. and Ahrens T. J. (1998) Shock wave equations of state of chondritic meteorites. In *Shock Compression of Condensed Matter–1997* (S. C. Dandekar et al., eds.), pp. 115–118. AIP Conference Proceedings 429, American Institure of Physics, New York.

Angel R. J., Chopelas A., and Ross N. L., (1992) Stability of high-density clinoenstatite at upper-mantle pressure. *Nature, 358,* 322–324.

Antoun T., Seaman L., Curran D. R., Kanel G. I., Razorenov S. V., and Utkin A. V., (2003) *Spall Fracture*. Springer-Verlag, New York. 404 pp.

Aramovich C. J., Sharp T. G., and Wolf G. (2003) The distribution and significance of shock-induced high-pressure minerals in chondrite Skip Wilson (abstract). In *Lunar and Planetary Science XXXIV,* Abstract #1355. Lunar and Planetary Institute, Houston (CD-ROM).

Asay J. R. (2002) Shock wave paradigms and new challenges. In *Shock Compression of Condensed Matter–2001* (M. D. Furnish et al., eds.), pp. 26–35. AIP Conference Proceedings 620, American Institute of Physics, New York.

Ashworth J. R. (1985) Transmission electron microscopy of L-group chondrites, 1. Natural shock effects. *Earth Planet. Sci. Lett., 73,* 17–32.

Baer M. R.(2000) Computational modeling of heterogeneous materials at the mesoscale. In *Shock Compression of Condensed Matter–1999* (M. Furnish et al., eds.), pp. 27–33. AIP Conference Proceedings 505, American Institute of Physics, New York.

Baer M. R. and Trott W. M. (2002) Mesoscale descriptions of shock-loaded heterogeneous porous materials. In *Shock Compression of Condensed Matter–2001* (M. D. Furnish et al., eds.), pp. 517–520. AIP Conference Proceedings 620, American Institute of Physics, New York.

Baer M. R. and Trott W. M. (2004) Mesoscale studies of shock loaded tin sphere lattices In *Shock Compression of Condensed Matter–2003* (M. D. Furnish et al., eds.), pp. 517–520. AIP Conference Proceedings 706, American Institute of Physics, New York.

Beck P., Gillet P., Gautron L., Danielle I., and El Goresy A. (2004) A new natural high-pressure aluminium-silicate in shocked martian meteorites. *Earth Planet. Sci. Lett., 219,* 1–12.

Beck P., Gillet Ph., El Goresy A., and Mostefaoui S. (2005) Timescales of shock processes in chondritic and martian meteorites. *Nature, 435,* 1071–1074.

Binns R. A. (1970) (Mg, Fe)$_2$SiO$_4$ spinel in a meteorite. *Phys. Earth Planet. Inter., 3,* 156–160.

Binns R. A., Davis R. J., and Reed S. B. J. (1969) Ringwoodite, natural (Mg, Fe)$_2$SiO$_4$ spinel in the Tenham meteorite. *Nature, 221,* 943–944.

Bischoff A. and Stöffler D. (1992) Shock metamorphism as a fundamental process in the evolution of planetary bodies: Information from meteorites. *Eur. J. Mineral., 4,* 707–755.

Bowden K. E. (2002) Effects of loading path on the shock metamorphism of porous quartz: An experimental study. Ph.D. thesis, University College London. 228 pp.

Bogard D. D. and Johnson P. (1983) Martian gases in an Antarctic meteorite? *Science, 221,* 651–654.

Brearley A. J., Rubie D. C., and Ito E. (1992) Mechanisms of the transformations between the α-polymorphs, β-polymorphs and γ-polymorphs of Mg_2SiO_4 at 15 GPa. *Phys. Chem. Minerals, 18,* 343–358.

Bundy F. P. and Kasper J. S. (1967) Hexagonal diamond — a new form of carbon. *J. Chem. Phys., 46,* 3437–3446.

Burnley P. C. and Green H. W. (1989) Stress dependence of the mechanism of the olivine spinel transformation. *Nature, 338,* 753–756.

Carter N. L., Raleigh C. B., and DeCarli P. S. (1968) Deformation of olivine in stony meteorites. *J. Geophys. Res., 73,* 5439–5461.

Chao E. C. T. (1967) Shock effects in certain rock-forming minerals. *Science, 156,* 192–202.

Chao E. C. T. (1968) Pressure and temperature history of impact metamorphosed rocks-based on petrographic observations. In *Shock Metamorphism of Natural Materials* (B. M. French and N. M Short, eds.), pp. 135–158. Mono, Baltimore.

Chen M. and El Goresy A. (2000) The nature of maskelynite in shocked meteorites: Not diaplectic glass but a glass quenched from shock-induced dense melt at high pressures. *Earth Planet. Sci. Lett., 179,* 489–502.

Chen M., Sharp T. G., El Goresy A., Wopenka B., and Xie X. (1996) The majorite-pyrope + magnesiowüstite assemblage. Constraints on the history of shock veins in chondrites. *Science, 271,* 1570–1573.

Chen M., Shu J. F., Xie X. D., and Mao H. K. (2003) Natural $CaTi_2O_4$-structured $FeCr_2O_4$ polymorph in the Suizhou meteorite and its significance in mantle mineralogy. *Geochim. Cosmochim. Acta, 67,* 3937–3942.

Chen M., El Goresy A., Frost D., and Gillet P. (2004a) Melting experiments of a chondritic meteorite between 16 and 25 GPa: Implication for Na/K fractionation in a primitive chondritic Earth's mantle. *Eur. J. Mineral., 16,* 203–211.

Chen M., El Goresy A, and Gillet P. (2004b) Ringwoodite lamellae in olivine: Clues to olivine-ringwoodite phase transition mechanisms in shocked meteorites and subducting slabs. *Proc. Natl. Acad. Sci. U.S., 101,* 15033–15037.

Consolmagno G. J. and Britt D. T. (1998) The density and porosity of meteorites from the Vatican collection. *Meteoritics & Planet. Sci., 33,* 1231–1241.

Courant R. and Friedrichs K. O. (1948) *Supersonic Flow and Shock Waves*. Interscience, New York.

Davis P. K. (1977) Effects of shock pressure on ^{40}Ar-^{39}Ar radiometric age determinations. *Geochim. Cosmochim. Acta, 41,* 195–205.

DeCarli P. S. (1979) Nucleation and growth of diamond in shock wave experiments. In *High Pressure Science and Technology, Vol. 1* (K. D. Timmerhaus and M. S. Barber, eds.), pp. 940–943. Plenum, New York.

DeCarli P. S. (1995) Shock wave synthesis of diamond and other phases. In *Mechanical Behavior of Diamond and Other Forms of Carbon* (M. D. Drory et al., eds.), pp. 21–31. Materials Research Society Symposium Proceedings 383, Materials Research Society.

DeCarli P. S. and Jamieson J. C. (1959) Formation of an amorphous form of quartz under shock conditions. *J. Chem. Phys., 31,* 1675–1676.

DeCarli P. S. and Jamieson J. C. (1961) Formation of diamond by explosive shock. *Science, 133,* 1821–1822.

DeCarli P. S., Bowden E., Jones A. P., and Price G. D. (2002a) Laboratory impact experiments versus natural impact events. In *Catastrophic Events and Mass Extinctions: Impacts and Beyond* (C. Koeberl and K. G. MacLeod, eds.), pp. 595–605. GSA Special Paper 356, Geological Society of America, Boulder.

DeCarli P. S., Bowden E., Sharp T. G., Jones A. P., and Price G. D. (2002b) Evidence for kinetic effects on shock wave propagation in tectosilicates. In *Shock Compression of Condensed Matter–2001* (M. D. Furnish et al., eds.), pp. 1381–1384. AIP Conference Proceedings 620, American Institute of Physics, New York.

De Carli P. S., Aramovich C. J., Xie Z., and Sharp T. G. (2004) Meteorite studies illuminate phase transition behavior of minerals under shock compression. In *Shock Compression of Condensed Matter–2003* (M. D. Furnish et al., eds.), pp. 1427–1430. AIP Conference Proceedings 706, American Institute of Physics, New York.

Dodd R. T. and Jarosewich E. (1979) Incipient melting in and shock classification of L-group chondrites. *Earth Planet. Sci. Lett. 59,* 335–340.

Duvall G. E. and Fowles G. R. (1963) Shock waves. In *High Pressure Physics and Chemistry, Vol. 2* (R. S. Bradley, ed.), pp. 209–291. Academic, London.

El Goresy A., Dubrovinsky L., Sharp T. G., Saxena S. K., and Chen M. (2000) A monoclinic polymorph of silica in the Shergotty meteorite. *Science, 288,* 37–55.

El Goresy A., Gillet P., Chen M., Künstler F., Graup G., and Stähle V. (2001) In situ discovery of shock-induced graphite-diamond transition in gneisses from the Ries Crater, Germany. *Am. Mineral., 86,* 611–621.

Fredriksson K. and DeCarli P. S. (1964) Shock emplaced argon in a stony meteorite I. *J. Geophys. Res., 69,* 1403–1406.

Fredriksson K., DeCarli P. S., and Aaramäe A (1963) Shock-induced veins in chondrites. In *Space Research III, Proceedings of the Third International Space Science Symposium* (W. Priester, ed.), pp. 974–983. North-Holland, Amsterdam.

Gasparik T. (1992) Melting experiments on the enstatite-pyrope join at 80–152 kbar. *J. Geophys. Res., 97,* 15181–15188.

Gillet P., Chen M., Dubrovinsky L., and El Goresy A. (2000) Natural $NaAlSi_3O_8$-hollandite in the shocked Sixiangkou meteorite. *Science, 287,* 1633–1636.

Goltrant O., Cordier P., and Doukhan J. C. (1991) Planar deformation features in shocked quartz: A transmission electron microscopy investigation. *Earth Planet. Sci. Lett., 106,* 103–155.

Goltrant O., Doukhan J. C., and Cordier P. (1992) Formation mechanisms of planar deformation features in naturally shocked quartz. *Phys. Earth. Planet. Inter., 74,* 219–240.

Gupta Y. M. (2002) The coupling between shock waves and condensed matter: Continuum mechanics to quantum mechanics. In *Shock Compression of Condensed Matter–2001* (M. D. Furnish et al., eds.), pp. 3–10. AIP Conference Proceedings 620, American Institute of Physics, New York.

Heinemann S., Sharp T. G., Seifert F., and Rubie D. C. (1997) The cubic-tetragonal phase transition in the system majorite ($Mg_4Si_4O_{12}$) — pyrope ($Mg_3Al_2Si_3O_{12}$), and garnet symmetry in the Earth's transition zone. *Phys. Chem. Minerals, 24,* 206–221.

Hemley R. J., Jephcoat A. P., Mao H. K., Ming L. C., and Manghani M. H. (1988) Pressure-induced amorphization of crystalline silica. *Nature, 334,* 52–54.

Heymann D. (1967) On the origin of hypersthene chondrites: Ages and shock effects of black chondrites. *Icarus, 6,* 189–221.

Hogrefe A., Rubie D. C., Sharp T. G., and Seifert F. (1994) Metastability of enstatite in deep subducting lithosphere. *Nature, 372,* 351–353.

Hörz F. (1968) Statistical measurements of deformation structures and refractive indices in experimentally shock loaded quartz. In *Shock Metamorphism of Natural Materials* (B. M French and N. M Short, eds.), pp. 243–253. Mono, Baltimore.

Huffman A. R., Brown J. M., Carter N. L., and Reimold W. U. (1993) The microstructural response of quartz and feldspar under shock loading at variable temperature. *J. Geophys. Res., 98,* 22171–22197.

Hugh-Jones T., Sharp T. G., Angel R., and Woodland A. (1996) The transition of orthoferrosilite to high-pressure *C2/c* clinoferrosilite at ambient temperature. *Eur. J. Mineral., 8,* 1337–1345.

Jeanloz R. (1980) Shock effects in olivine and implications for Hugoniot data. *J. Geophys. Res., 85,* 3163–3176.

Kerschhofer L., Sharp T. G., and Rubie D. C. (1996) Intracrystalline transformation of olivine to wadsleyite and ringwoodite under subduction zone conditions. *Science, 274,* 79–81.

Kerschhofer L., Dupas C., Liu M., Sharp T. G., Durham W. B., and Rubie D. C. (1998) Polymorphic transformations between olivine, wadsleyite and ringwoodite: Mechanisms of intracrystalline nucleation and the role of elastic strain. *Mineral. Mag., 62,* 617–638.

Kerschhofer L., Rubie D. C., Sharp T. G., McConnell J. D. C., and Dupas-Bruzek C. (2000) Kinetics of intracrystalline olivine-ringwoodite transformation. *Phys. Earth Planet. Inter., 121,* 59–76.

Kieffer S. W. (1971) Shock metamorphism of the Coconino sandstone at Meteor Crater. Arizona. *J. Geophys. Res., 76,* 5449–5473.

Kieffer S. W., Phakey P. P., and Christie J. M. (1976) Shock proc-

esses in porous quartzite: Transmission electron microscope observations and theory. *Contrib. Mineral. Petrol., 59,* 41–93.

Koeberl C., Masaitis V. L., Shafranovsky G. I., Gilmour I., Langenhorst F., and Schrauder M. (1997) Diamonds from the Popigai impact structure. *Geology, 25,* 967–970.

Kubo T., Ohtani E., Kato T., Morishima H., Yamazaki D., Suzuki A., Mibe K., Kikeegawa T., and Shimomura O. (1998a) An in situ X-ray diffraction study of the α-β transformation kinetics of Mg_2SiO_4. *Geophys. Res. Lett., 25,* 695–698.

Kubo T., Ohtani E., Kato T., and Fujino K. (1998b) Experimental investigation of the α-β transformation in San Carlos olivine single crystal. *Phys. Chem. Mineral., 26,* 1–6.

Langenhorst F. and Poirier J. P. (2000a) Anatomy of black veins in Zagami: Clues to the formation of high-pressure phases. *Earth Planet. Sci. Lett., 184,* 37–55.

Langenhorst F. and Poirier J. P. (2000b) 'Eclogitic' minerals in shocked basaltic meteorite. *Earth Planet. Sci. Lett., 176,* 259–265.

Langenhorst F., Joreau P., and Doukhan J. C. (1995) Thermal and shock metamorphism of the Tenham chondrite: A TEM examination. *Geochim. Cosmochim. Acta, 59,* 1835–1845.

Leroux H. (2001) Microstructural shock signatures of major minerals in meteorites. *Eur. J. Mineral., 13,* 253–272.

Lipschutz M. E. (1968) Shock effects in iron meteorites: A review. In *Shock Metamorphism of Natural Materials* (B. M. French and N. M. Short, eds.), pp. 571–599. Mono, Baltimore.

Liu M., Kerschhofer L., Mosenfelder J., and Rubie D. C. (1998) The effect of strain energy on growth rates during the 4 olivine-spinel transformation and implications for olivine metastability in subductoing slabs. *J. Geophys. Res., 103,* 23897–23909.

Madon M. and Poirier J. P. (1980) Dislocations in spinel and garnet high-pressure polymorphs of olivine and pyroxene: Implications for mantle mineralogy. *Science, 207,* 66–68.

Madon M. and Poirier J. P. (1983) Transmission electron microscope observation of α, β, γ $(Mg,Fe)_2SiO_4$ in shocked meteorites: Planar defects and polymorphic transitions. *Phys. Earth Planet. Inter., 33,* 31–44.

Mason B., Nelen J., and White S. J. Jr. (1968) Olivine-garnet transformation in a meteorite. *Science, 160,* 66–67.

McQueen R. G. (1964) Laboratory techniques for very high pressures and the behavior of metals under dynamic loading. In *Metallurgy at High Pressures and High Temperatures* (K. S. Gschneider et al., eds.), pp. 44–132. Gordon and Breach, New York.

McQueen R. G., Marsh S. P., Taylor J. W., Fritz J. N., and Carter W. J. (1970) The equation of state of solids from shock wave studies. In *High-Velocity Impact Phenomena* (R. Kinslow, ed.), pp. 530–568. Academic, New York.

Melosh H. J. (1989) *Impact Cratering: A Geologic Process.* Oxford Univ., New York. 245 pp.

Meyers M. A. (1994) *Dynamic Behavior of Materials.* Wiley and Sons, New York. 688 pp.

Migault A. (1998) Concepts of shock waves. In *Impacts on Earth* (D. Benest and C. Froeshlé, eds.), pp. 79–112. Springer-Verlag, Berlin.

Milton D. J. and DeCarli P. S. (1963) Maskelynite: Formation by explosive shock. *Science, 147,* 144–145.

Mori H. (1994) Shock-induced phase transformations on the Earth and planetary materials. *J. Mineral. Soc. Japan, 23,* 171–178.

Mori H. and Takeda H. (1985) Magnesiowüstite in a shock-produced vein of the Tenham chondrite (abstract). In *Lunar and Planetary Science XVI,* pp. 579–598. Lunar and Planetary Institute, Houston.

Mosenfelder J. L., Marton F. C., Ross C. R. II, Kerschhofer L., and Rubie D. C. (2001) Experimental constraints on the depth of olivine metastability in subducting lithosphere. *Phys. Earth Planet. Inter., 127,* 165–180.

Nesterenko V. F. (2001) *Dynamics of Heterogeneous Materials.* Springer-Verlag, New York. 510 pp.

Ohtani E., Kimura Y., Kimura M., Takata T., Kondo T., and Kubo T. (2004) Formation of high-pressure minerals in shocked L6 chondrite Yamato 791384: Constraints on shock conditions and parent body size. *Earth Planet. Sci. Lett., 227,* 505–515.

Panero W. R., Benedetti L. R., and Jeanloz R. (2003) Equation of state of stishovite and interpretation of SiO_2 shock-compression data. *J. Geophys. Res., 108,* B012015, doi:10.1029/2001JB001663.

Pepin R. O., Reynolds J. H., and Turner G. (1964) Shock emplaced argon in a stony meteorite II. *J. Geophys. Res., 69,* 1406–1411.

Porter D. A. and Easterling K. E. (1978) Dynamic studies of the tensile deformation and fracture of pearlite using high-resolution 200-KV SEM. *Scandinav. J. Metall., 7,* 55–56.

Price G. D. (1983) The nature and significance of stacking-faults in wadsleyite, natural beta-$(Mg,Fe)_2SiO_4$ from the Peace River meteorite. *Phys. Earth Planet. Inter., 33,* 137–147.

Price G. D., Putnis A., and Agrell S. O. (1979) Electron petrography of shock-produced veins in the Tenham chondrite. *Contrib. Mineral. Petrol., 71,* 211–218.

Price G. D., Putnis A., and Smith D. G. W. (1982) A spinel to β-phase transformation mechanism in $(Mg,Fe)_2SiO_4$. *Nature, 296,* 729–731.

Price G. D., Putnis A., Agrell S. O., and Smith D. G. W. (1983) Wadsleyite, natural beta-$(Mg,Fe)_2SiO_4$ from the Peace River meteorite. *Can. Mineral., 21,* 29–35.

Putnis A. and Price G. D. (1979) High-pressure $(Mg, Fe)_2SiO_4$ phases in the Tenham chondritic meteorite. *Nature, 280,* 217–218.

Rubie D. C. (1993) Mechanisms and kinetics of reconstructive phase transformations in the Earth's mantle. In *Short Courses Handbook on Experiments at High Pressure and Applications to the Earth's Mantle, Vol. 21* (R. W. Luth, ed.), pp. 247–303. Mineralogical Association of Canada, Edmonton.

Rubie D. C. and Ross C. R. (1994) Kinetics of the olivine-spinel transformation in subducting lithosphere: Experimental constraints and implications for deep slab processes. *Phys. Earth Planet. Inter., 86,* 223–241.

Rubin A. E. (2004) Postshock annealing and postannealing shock in equilibrated ordinary chondrites: Implications for the thermal and shock histories of chondritic asteroids, *Geochim. Cosmochim. Acta, 68,* 673–689.

Rubin A. E. (2005) What heated the asteroids? *Sci. Am., 285(5),* 81–87.

Schmitt D. R. and Ahrens T. J. (1983) Temperatures of shock-induced shear instabilities and their relation to fusion curves. *Geophys. Res. Lett., 10,* 1077–1080.

Schmitt R. T. (2000) Shock experiments with the H6 chondrite Kernouvé: Pressure calibration of microscopic shock effects. *Meteoritics & Planet. Sci., 35,* 545–560.

Scott E. R. D., Keil K., and Stöffler D. (1992) Shock metamorphism of carbonaceous chondrites. *Geochim. Cosmochim. Acta, 56,* 4281–4293.

Sears D. W. and Dodd R. T. (1988) Overview and classification

of meteorites. In *Meteorites and the Early Solar System* (J. F. Kerridge and M. S. Matthews, ed.), pp. 3–31. Univ. of Arizona, Tucson.

Sharp T. G. and Rubie D. C. (1995) Catalysis of the olivine to spinel transformation by high clinoenstatite. *Science, 269,* 1095–1098.

Sharp T. G., Lingemann C. M., Dupas C., and Stöffler D. (1997) Natural occurrence of $MgSiO_3$-ilmenite and evidence for $MgSiO_3$-perovskite in a shocked L chondrite. *Science, 277,* 352–355.

Sharp T. G., El Goresy A., Wopenka B., and Chen M. (1999) A post-stishovite SiO_2 polymorph in the meteorite Shergotty: Implications for impact events. *Science, 284,* 1511–1513.

Smith J. V. and Mason B. (1970) Pyroxene-garnet transformation in Coorara meteorite. *Science, 168,* 832.

Spray J. G. (1999) Shocking rocks by cavitation and bubble implosion. *Geology, 27,* 695–698.

Stöffler D. (1972) Deformation and transformation of rock-forming minerals by natural and experimental shock processes: I. Behavior of minerals under shock compression. *Fortsch. Mineral., 49,* 50–113.

Stöffler D. (1974) Deformation and transformation of rock-forming minerals by natural and experimental shock processes: II. Physical properties of shocked minerals. *Fortsch. Mineral., 51,* 256–289.

Stöffler D., Bischoff A., Buchwald V., and Rubin A. E. (1988) Shock effects in meteorites. In *Meteorites and the Early Solar System* (J. F. Kerridge and M. S. Matthews, ed.), pp. 165–202. Univ. of Arizona, Tucson.

Stöffler D., Keil K., and Scott E. R. D. (1991) Shock metamorphism of ordinary chondrites. *Geochim. Cosmochim. Acta, 55,* 3845–3867.

Taylor G. J. and Heymann D. (1969) Shock, reheating, and the gas retention ages of chondrites. *Earth Planet. Sci. Lett., 7,* 151–161.

Tomeoka K., Yamahana Y., and Sekine T. (1999) Experimental shock metamorphism of the Murchison CM carbonaceous chondrite. *Geochim. Cosmochim. Acta, 63,* 3683–3703.

Tomioka N. and Fujino K. (1997) Natural $(Mg,Fe)SiO_3$-ilmenite and -perovskite in the Tenham meteorite. *Science, 277,* 1084–1086.

Tomioka N., Mori H., and Fujino K. (2000) Shock-induced transition of $NaAlSi_3O_8$ feldspar into a hollandite structure in a L6 chondrite. *Geophys. Res. Lett., 27,* 3997–4000.

Tschermak G. (1872) Die meteoriten von Shergotty und Goalpur. *Sitzber. Akad. Wiss. Wien Math.-naturw., Kl. Abt I, 65,* 122–146.

Van Schmus W. R. and Ribbe P. H. (1968) The composition and structural state of feldspar from chondritic meteorites. *Geochim. Cosmochim. Acta, 32,* 1327–1342.

Walsh J. M. and Christian R. H. (1955) Equation of state of metals from shock wave measurements. *Phys. Rev., 97,* 1544–1556.

Wiens R. C. and Pepin R. O. (1988) Laboratory shock emplacement of noble gases, nitrogen, and carbon dioxide into basalt, and implications for trapped gases in shergottite EETA 79001. *Geochim. Cosmochim. Acta, 52,* 295–307.

Williams Q. and Jeanloz R. (1989) Static amorphization of anorthite at 300 K and comparison with diaplectic glass. *Nature, 338,* 413–415.

Xie Z. (2003) Transmission electron microscopy study of high pressure phases in the shock-induced melt veins of L chondrites: Constraints on the shock pressure and duration. Ph.D. thesis, Arizona State Univ., Tempe. 149 pp.

Xie Z. and Sharp T. G. (2000) Mineralogy of shock-induced melt veins in chondrites as a function of shock grade (abstract). In *Lunar and Planetary Science XXXI,* Abstract #2065. Lunar and Planetary Institute, Houston (CD-ROM).

Xie Z. and Sharp T. G. (2003) TEM observations of amorphized silicate-perovskite, akimotoite, and Ca-rich majorite in a shock-induced melt vein in the Tenham L6 chondrite (abstract). In *Lunar and Planetary Science XXXIV,* Abstract #1469. Lunar and Planetary Institute, Houston (CD-ROM).

Xie Z. and Sharp T. G. (2004) High-pressure phases in shock-induced melt veins of the Umbarger L6 chondrite: Constraints on shock pressure. *Meteoritics & Planet. Sci., 39,* 2043–2054.

Xie Z., Tomioka N., and Sharp T. G. (2002) Natural occurrence of Fe_2SiO_4-spinel in the shocked Umbarger L6 chondrite. *Am. Mineral., 87,* 1257–1260.

Xie Z., Sharp T. G., and DeCarli P. S. (2003) Estimating shock pressures from high-pressure minerals in shock-induced melt veins of the chondrites (abstract). In *Lunar and Planetary Science XXXIV,* Abstract #1280. Lunar and Planetary Institute, Houston (CD-ROM).

Xie Z., Sharp T. G., and DeCarli P. S. (2005) High pressure phases in a shock-induced melt vein of Tenham L6 chondrite: Constraints on shock pressure and duration. *Geochim. Cosmochim. Acta,* in press.

Zener C. and Hollomon J. H. (1944) Effect of strain rate on plastic flow of steel. *J. Appl. Phys., 15,* 22–32.

Zhang J. and Herzberg C. (1994) Melting experiments on anhydrous peridotite KLB-1 from 5.0 to 22.5 GPa. *J. Geophys. Res., 99,* 17729–17742.